Bi-monthly • July - August • 2017

ISSN: 0976-2108

BARC NEWSLETTER

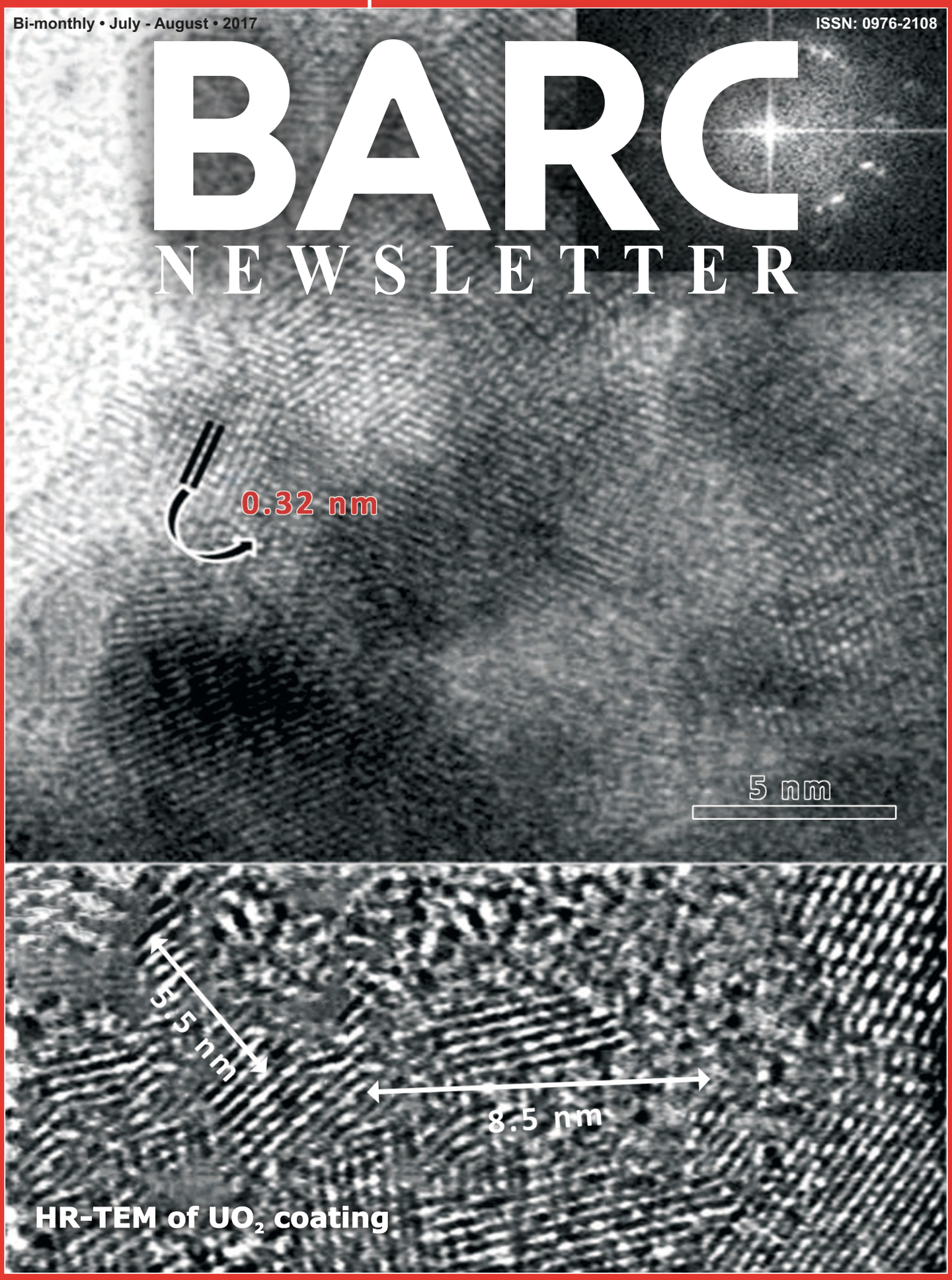

HR-TEM of UO_2 coating

CONTENTS

1st Al-Si ingot made in ISM Facility being handed over to the Nuclear Fuel Group
(from L to R: Dr. J.G. Shah, Head, PSDD, Dr. G. Sugilal, Head, TDDS, Shri K. Aggarwal, AD, NRG and Shri V.K. Bhasin, AD, NFG)

Development of Induction Skull Melting Facility for Al-Si Alloy Production

Technology Development Division
Nuclear Recycle Group

Induction Skull Melting (ISM) is an advanced technology used for melting highly reactive metals such as titanium, zirconium, etc. In ISM, the metallic charge is melted in a water-cooled segmented copper crucible by electromagnetic induction. The skull formed between the crucible and the melt prevents any contamination of the product. By virtue of high temperature availability, strong electromagnetic stirring and long crucible life without product contamination, Induction Skull Melting technology can be used for producing various metals and alloys with high purity and homogeneity. Technology Development Division, Nuclear Recycle Group, indigenously developed an Induction Skull Melting Facility in view of various important applications in frontier areas of material research, development and production [BARC Newsletter, Nov-Dec, 2015, 50-55].

The ISM Facility was operated on trial basis for one year to demonstrate consistent and reliable operation. During the trial operation, ISM technology was successfully used for the production of boron containing alloys. By virtue of strong electromagnetic stirring, boron gets uniformly distributed. ISM technology is also useful for producing alloys from their constituent metals having great differences in their densities and melting points. This was demonstrated by producing an alloy of Nickel, Chromium, Molybdenum and Tungsten using the ISM Facility. Based on the successful trial operations, BARC Safety Council granted regulatory clearance for one year regular operation of the ISM Facility.

Induction Skull Melting Facility in Nuclear Recycle Group, BARC

First batch of Al- Si alloy produced in the ISM Facility

Al-Si mother alloy was also successfully melted and homogenized in the ISM Facility to meet required levels of purity and homogeneity. The ISM Facility is now under regular operation for the production of Aluminium-Silicon alloy in order to meet the requirements of NFG. Production of 1st batch of Aluminium-Silicon alloy (10 ingots) has been completed and the consignment has been shipped to NFG.

Development of Driver and Controller for Laser Diode Modules

Amresh Kumar Jha and Supratim Majumdar
Electronics & Instrumentation Group

Laser diode modules are being used for interferometry and sensor development in Advanced Technology Systems Section (ATSS) and Precision Engineering Division (PED). Laser diode modules come in different packages and may contain a monitor photo diode, a thermistor and a Thermo Electric Cooler (TEC) apart from the laser diode.

A driver-and-controller unit has been developed to drive the laser diode either in constant current or in constant power mode and in order to maintain the module temperature at a set value. The system uses a high precision programmable current source (Range: 0-750mA in 1mA steps) to drive the laser diode. The range and step size can be changed. Laser module temperature can however be varied from 15°C to 34°C in steps of 1°C with the accuracy of ±0.2°C. User selectable current limit or power limit and slow start feature ensure safety of the laser diode. User can navigate through the menus on the user console to set the mode of operation and parameters like module temperature, current or power limit etc.

Photograph of one of the units delivered to PED

Development of Hull Waste Batching System for Integrated Nuclear Recycle Plant

Chhag Mayur N., Haldar K. K., Haneef K. K. M. and K. Ravi
Nuclear Recycle Board

Abstract

Hull compaction facility is being designed for the first time in India. Hull batching is the first processing step in hull compaction facility of Integrated Nuclear Recycle Plant (INRP). As INRP is a high throughput plant, the generation of hull waste will be in large quantity. The hull waste is associated with high level radioactivity having long lived radio isotopes. Hence, there is a need for volume reduction of these wastes to minimise the long term storage space requirement at geological repository and at in-plant engineered storage.

Various types of feeder designs have been studied before finalising the type of basic feeder equipment for batching system. As the batching system handles high level of radioactivity associated with alpha contaminations, it is required to be highly reliable and amenable for easy maintenance in addition to performing its primary batching functions. A gravimetric vibratory feeder based hull batching system has been developed after extensive mock up trials.

Introduction

Hull waste is a structural part of un-dissolved fuel assembly that is separated during dissolution process of chopped spent fuel in reprocessing facilities. They are associated with high level of radioactivity along with alpha contaminations which contains zircoloy fines, residual fission products and heavy metals. The hulls are hollow cylindrical waste, which occupy huge volume. A presently operating plant typically generates hull waste in the order of 30 cubic meters per year, which are being stored in storage facility without any compaction. As the upcoming INRP is a large capacity plant; the volume of hull waste generated will be very high, in the order of 160 cubic meters per year. Therefore, compaction of these hull wastes was felt necessary.

Hull batching is an important part and the first step in hull processing. An objective of the hull batching process is to use standard canister as container for hull wastes that is finalised for Vitrified Waste Product so as to have identical design for storage locations and material handling/ remote handling systems for different high active solid waste products at engineered storage facilities as well as at geological repositories. The hull batching system is designed to transfer hull wastes from a hull drum, containing one batch of spent fuel hulls into 8 nos. of smaller sized cans. The basis of selection of dimensions of the can is to accommodate compacted discs into the standard sized canisters.

As the batching system is being designed for this application for the first time, mock ups trials were carried out to establish their reliability and performance of the system.

Studies of Various Bulk Solid Feeders

The equipment for batching system of this kind was being developed for the first time indigenously. This required design innovations, literature survey and trial mock ups for the equipment before finally being considered for inducting in INRP. Various types[1] of feeder designs, which are commercially available for bulk solids, have been studied in detail. Also, feedbacks from different types of commercial bulk solid feeders were taken from industries/ users. They are also studied with respect to their suitability in adopting in radiation environment. High system reliability and easy maintenance are the critical requirements of the feeder system in addition to performance of conventional feeder functions. Important criteria for selection of feeders for hull batching system are briefly listed below:

a) Uninterrupted and reliable flow of hull pieces from the feeder tray
b) Achieving desired flow rate and accuracy of the flow
c) Reliability of system
d) Immediate start/stop after switching
e) Easy/remote replacement for maintenance prone parts
f) Suitability in high radiation environment
g) Design for control of contamination spread
h) Easy to decontaminate
i) Sizes and type of hull waste

Various commonly used feeders in the industries are screw feeders, rotary valves, vibratory feeders, belt feeders, flexible wall hoppers, etc. Basically, feeders are used to modulate and control the mass flow rates of solids. The pros and cons of each type of feeder were analysed. Finally, a gravimetric electromagnetic vibratory feeder was selected for detailed studies for incorporating it in a batching system and its amenability for remote maintenance. The electromagnetic vibratory feeder has several advantages over other types of bulk solid flow equipment[2]. First, it is extremely rugged and simple in construction. Second, it can be enclosed to eliminate contamination spread from hulls. Third, it can be made amenable for remote maintenance.

Design Concept

Feeder is used to control discharge from a system. Control involves not only stopping and starting flow but also metering the rate of discharge. Vibratory feeder controls the discharge using vibrator. An electro-magnetic vibrator is selected for hull batching system owing to its high reliability and accuracy of flow. This vibrator is a spring-mass oscillation system using electro-magnets that exploit the resonance of the oscillation. If the system is stimulated, it continues to oscillate with its natural frequency, with decaying amplitude depending on its attenuation properties.

A gravimetric vibratory feeder used for the batching system provides closed loop feedback information about the actual weight of the hull pieces being discharged into the destination container and modulate the feed for coarse and fine feed accordingly. It uses vibrations and gravity both to move the materials. Gravity determines the direction of the flow and vibrations controls the feed rate of the materials. The bulk hull pieces are delivered into the hopper from the top and pour the hull pieces from exit hopper through feeder in a controlled fashion. Basic principle of the feeder is that when the magnet receives power, vibration occurs because a pulsating magnetic field is established between the armature and the magnet. There are leaf springs provided in the feeder which permit the armature to move toward and away from the magnet, which imparts the vibration to the tray that ultimately moves the materials.

Hull compaction facility comprises of facilities for hull receipt, hull batching, hull drying, compaction of cans, compacted discs filling into standard canisters, welding of canisters with lids, contamination check/decontamination of canisters, and interim storage in shielded vaults. The block diagram depicting major process steps in the facility is shown in Fig.1 below:

The batching system is planned to be installed inside a shielded cell, called batching cell. The cell is provided with various remote viewing and handling arrangements to carry out the batching operation remotely. Hull waste drums are received in hull compaction facility from reprocessing block. The drum is brought to the batching cell through underground shielded tunnel by a remotely operated trolley. Empty cans are feed to the cell through external transfer drawer through remotely operated can transfer trolley. A load cell based weighing is inbuilt in the trolley trough, which is integrated with the batching system for closed feedbacks through controller. Position accuracy of the trolley is achieved by a shaft encoder/proximity switches. These cans are provided with corrugations on shells for easy compaction. The cell is provided with in-cell crane, master slave manipulators, radiation shielding windows, cameras, grapples, electrically operated can transfer trolleys and external transfer drawers for remote viewing and handling of cans. All the drives are kept outside the cell through stepped plugs type embedded parts in shielded walls. The batching cell is surrounded by operating galleries for operation within the cell.

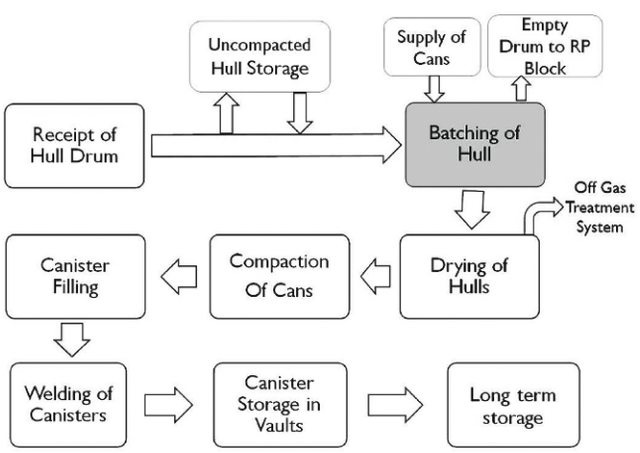

Fig. 1: Block diagram of hull compaction facility

Design Features

The vibratory feeder type batching system consists mainly of 1) Main hopper 2) Drum tilting assembly 3) Electromagnetic Vibrator 4) Vibratory tray 5) Exit hopper drain 6) Outer casing. The drum tilting assembly has rotating cage structure, which receives hull drum from top. It has a locking strip for locking in position of the hull drum. The tilting of the drum at desired angle is achieved by means of an electrical motor drive. The hull pieces are poured from the drum directly into the hopper unit. The main hopper bottom exit diameter is chosen to avoid arching of hull pieces. At the exit of the hopper, there is a vibratory tray, which will feed the hull pieces into the can through exit hopper drain. A tapered guided feeder tray of overall size 400mm (W) x 1400mm (L) x 200mm (H) is provided. The feeder tray size is worked out based on the requirement of buffer storage capacity for 1 batch operation of hull pieces. An electromagnetic vibrator is directly attached to the feeder tray with standard below deck mounting arrangement[3]. The vibrator motor rating is 0.4 KW. The vibrator is variable amplitudes and fixed vibration frequency type. The feeder tray oscillates 3000 oscillations per minute at 50 Hz-mains. Working stroke of the vibrator and hence the throughput can be adjusted during operation from very low to 100 % by changing the voltage from the controller. The normal working stroke for 100% operating flow is adjusted at 2 mm where 90% of the flow takes place, while last 10% of the flow is with low amplitude for finer flow to achieve desired batching accuracy of less than 0.5%. One cycle of batching is corresponding to 30 Kg of hull pieces. Coil spring isolators are planned between the support and feeder tray. Discharge mass flow rate of the hull pieces of the batching system is 400 Kg/hr. Main-stay material of construction for various parts of the batching system is austenitic stainless steel grade 304L. Major parts of the vibrator are also constructed from stainless steel material. A Schematic of the hull batching system is given in Fig. 2.

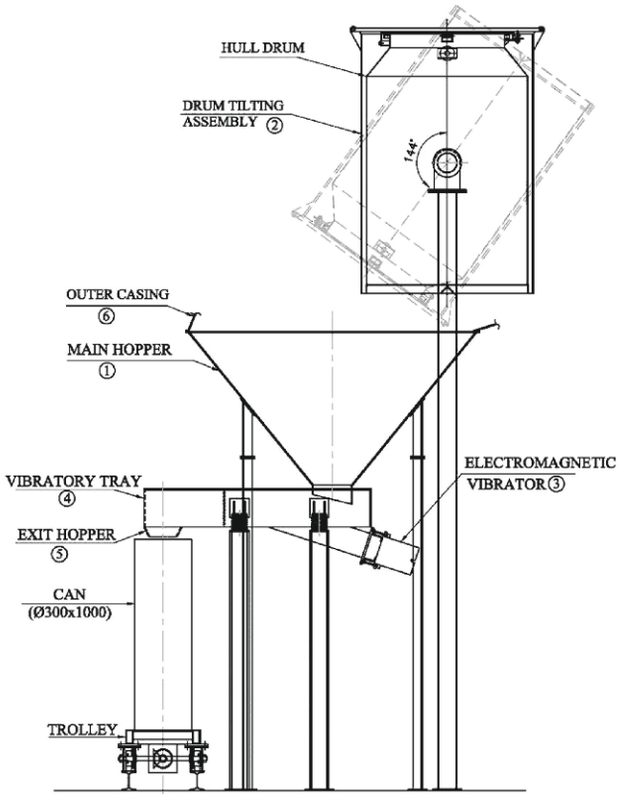

Fig. 2: Schematic of Hull batching system

This system is a low-maintenance, continuous duty, no-wear operation and high reliability type. The vibrator unit consisting mainly of electromagnet, leaf springs and masses, which are housed in a stainless steel casing with ingress protection rating as IP 65 class. The vibrator unit is attached with the feeder tray by means flange connection. In case of failure of the vibrator module, it can be detached remotely from the feeder tray with the help of remote gadgets specifically designed for this purpose like special guide tools, impact wrench, etc. and using in-cell crane available in the cell. Electrical cables to the vibrator are having quick connection type connectors. An active maintenance area is provided adjacent to the batching cell for any contact maintenance.

Hull drum is brought to the hull tilting arrangement by in-cell crane and grapples. A drum tilting frame with drum locking arrangement is provided. With the help of mechanised lever arrangement, the drum is locked in the position. The hopper lid will be closed before tilting and off-gas is turned-on to maintain a negative pressure inside the hopper. The drum is tilted in a controlled fashion into the hopper so that the bulk hull pieces will fall into the hopper as per the quantity of the batch size. The drum tilting is done by using an electric motor with sector gear arrangement, which is kept outside the cell. A pour point of the tray has been provided with open/close type gate, having diameter of 175mm. This gate will avoid any unwanted fall of the hull piece from pour point by gravity after the system is switched off. The hopper angle and size of outlets of batching system are finalised based on the hull material properties. Hopper design is carried out achieve mass flow mode. Bottom opening is sized to prevent mechanical interlocking of hull pieces. A floor tray is also planned below the batching unit, where any accidental fall of hull pieces will be collected.

Inactive dummy hull pieces have been used in the trials. An existing commercial feeder of similar capacity has been used for the purpose. The feeder was tested extensively for studying its performance. Around 6000 nos. of dummy hull pieces, corresponding to 30 Kg of hulls of 1 batch were used for the testing purpose. The feeder was operated in a batch mode. The feeder tray vibration frequency was 3000 oscillations per minutes. It was observed that the hulls of one can quantity, i.e. 30 Kg were collected inside the existing box within 5 minutes. During trials, a batching accuracy of better than 0.5 % by weight was achieved.

Control Logics and Safety Interlocks

The system operation is controlled by stand-alone Programmable Logic Control system, which is kept at operating gallery outside the cell. The control access is provided from local control panels at PLC within the plant and also important signals are duplicated at central control room of INRP. Various safety interlocks are provided to ensure availability of empty can on the trolley, Positioning of can trolley below pour point, Closure of drum locking strip & hopper lid, Start of Off-gas system etc. Also fine and coarse flow by Vibrators will be based on feedback from load cell based weighing system. Close of batching operation will be based on feedback of the weight of hulls being filled in the can from load cell.

Conclusion

Various commercially available bulk solid feeders have been studied and feedbacks from industries have been taken for selecting a type of feeder to be incorporated in the batching system. A gravimetric electromagnetic vibratory feeder based batching system has been developed. Flow parameters have been arrived after extensive mock up trials on the existing commercial feeder, carried out at vendor's works. Issues of maintenance and spread of contamination have been taken care in design of the system.

References

1. McGlinchey, Don. *Bulk Solid Handlings: Equipment selection and operation*, Blackwell Publishing, 2008.
2. Carson, John W., Petro, Greg. "How to Design Efficient and Reliable Feeders for Bulk Solids", Jenike & Johanson Inc., Flow of Solids Newsletters.
3. Cleveland Vibratory Feeder Catalog, "http://www.ipcd-inc.com/conveyors/vibratory/".

^{131}I Labeled Lipiodol Injection: A Cost Effective Alternative for Liver Cancer Treatment

Archana Mukherjee, Rajwardhan Ambade, Suresh Subramanian, Bhaurao Avhad, Ashutosh Dash and Aruna Korde
Radiopharmaceutical Division, Radiochemistry & Isotope Group

Global incidence of Hepatocellular carcinoma (HCC) is reported to be more than 1 million patients per year. In Asia and Africa, it is the most frequent cause of cancer-induced deaths. Due to the late appearance of symptoms and poor patient prognosis, more than 95% of patients do not survive five years past the initial diagnosis. Resective surgery, systemic chemotherapy and external beam radiotherapy have proven singularly ineffective for treatment of the disease in terms of survival benefit.

Trans-arterial chemo-embolization (TACE) using drugs like cisplatin, doxorubicin, methotrexate, paclitaxel has been employed in conjunction with Lipiodol for locoregional therapy. TACE involves administration of drugs intra-arterially for preferential localization in regions of tumor as majority of normal hepatic blood supply is via the portal vein and neo-angiogenic vessels are primarily connected to the hepatic artery as shown in Fig 1.

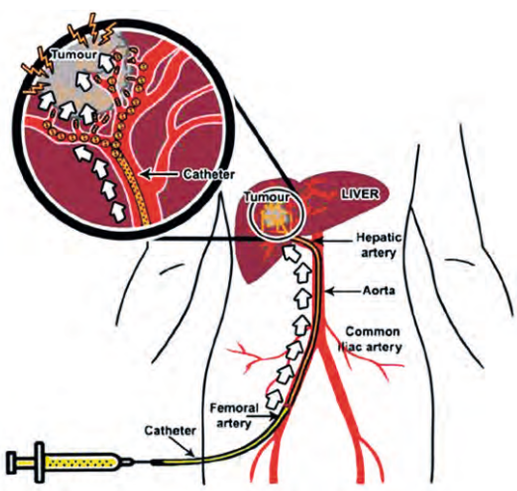

Fig 1.: Schematic representation of transarterial radioembolization (TARE) procedure

In TACE, Lipiodol serves as both drug carrier and embolizing agent. Intra-vasal retention of Lipiodol leads to starvation of tumor cells of nutrient and oxygen supply and deliver high doses of the drug(s) loco-regionally, which provides greater chemotherapeutic effect than by the systemic route. Embolization in conjunction with a radiotherapy agent, is called radio-embolization.There are two main categories of radio-embolic agents approved for clinical use. First category is based on micron-range particulates that encapsulate or adsorb therapeutic radionuclides, like ^{90}Y-bearing glass spheres (Therasphere®) and polymeric selective internal radiation spheres(SIR-spheres®).

Although Therasphere and SIR -spheresare are being used worldwide, their exorbitant cost is a major limitation for their wider use in developing countries like India. Second category is Lipiodol or related embolic substances tagged with therapeutic radionuclide.

Lipiodol or Ethiodised oil is a naturally iodinated fatty acid ethyl ester of poppy seed oil (37%w/w of iodine). It is employed as a magnetic resonance imaging (MRI) contrast agent for the liver and has also been labeled with therapeutic radionuclides such as ^{131}I and ^{188}Re for HCC treatment. Isotopic exchange is used to label iodine rich Lipiodol with ^{131}I to prepare radioiodinated Lipiodol, while ^{188}Re-labeled 4-hexadecyl-1-2, 9, 9-tetramethyl-4, 7-diaza-1, 10-decanethiol (HDD) is dispersed in Lipiodol for preparation of ^{188}Re-labeled radioembolizing agent.[123]

I-131, radioisotope is indigenously available in sufficient quantities at a very lost cost due to its reactor production route and dry distillation processing method as compared to generator produced ^{90}Y and ^{188}Re.[4] ^{131}I labeled Lipiodol can be

Table 1: Comparison of Radiopharmaceuticals for Transarterial radioembolization

Radiopharmaceuticals	Glass spheres (Therasphere®)	Polymeric SIR-spheres®.	^{188}Re-HDD-Lipiodol	^{131}I-labeled Lipiodol
Radioisotope	^{90}Y	^{90}Y	^{188}Re	^{131}I
Nuclear Emissions	$E_{\beta max}$: 2.28MeV	$E_{\beta max}$: 2.28MeV	$E_{\beta max}$: 2.12 MeV, 1.97 MeV Eγ: 155 keV	$E_{\beta max}$:610 KeV Eγ: 364KeV; 637 keV
Half Life	64.1h	64.1h	17 h	8 days
Production of isotope	^{90}Sr/^{90}Y Generator	^{90}Sr/^{90}Y Generator	^{188}W/^{188}Re Generator	Reactor
Material	Glass	Resin	Oil	Oil
Cost per patient dose	~ 5 lakhs	~ 5 lakhs	~ 2 lakhs	40,000/-
Availability	Imported	Imported	Imported	BARC/ BRIT product

easily prepared and supplied from a centralized radiopharmacy owing to suitable half-life of ^{131}I, allowing convenient logistics of production and quality control checks prior to patient administration.

There is a demand from Nuclear medicine fraternity for ^{131}I labeled Lipiodol if supplied as a cost effective, ready-to-use radiopharmaceutical. The patient dose preparation of ^{131}I labeled Lipiodol requires high amounts of initial activity (>3.7GBq) of ^{131}I. The high energy gamma radiations (637 KeV, ~7% abundance & $E_{\beta max}$: 610 KeV)of ^{131}I pose considerable safety related limitations for radiolabeling. Hence, a semi-automated modular system was designed and fabricated to ensure operator safety as well as pharmaceutical purity and safety of the product.

Design

Photograph of semi-automated module for production of patient dose of ^{131}I-Lipiodol and control panel is depicted in Fig 2.The module holds two lead pots of 30mm thickness. The lead pot containing Na^{131}I can easily slide on the base plate of the module and the radioactivity vial gets firmly held with the help of a precisely designed bottle guard plate for safe operations. The reaction vessel assembly is enclosed in a silicon glycerin bath, fitted at rear end of the base plate of the module.

Precise addition of reagents to vials as well as all transfers of reagents are carried out remotely. Inert nitrogen gas of high purity is used for pressurizing vessels. Tefzel tubings compatible with organic solvents are used for transfer of reagents which are connected to solenoid valves mounted on plate and connected to junction box. Heating of reaction vessel is carried out using thermocouple with display of temperature.

The module is placed inside locally designed and fabricated shielded facility similar to commercially available mini hot cell with adequate lead shielding having negative pressure and charcoal filters fitted at release duct. For external surface sterilization of this set up ultraviolet light is installed and kept on for minimum three hours prior to synthesis. Electrical valve operations and heating controls are placed separately on control panel, which are operated manually by simple on/off switch away from module. Valve operation sequence was standardized based on optimized reaction parameters. Radiation field, air activity and activity released through charcoal trap were monitored during all operations. Several batches of ^{131}I labeled Lipiodol were prepared using standardized operating protocol.[5]

Radiosynthesis

Isotope exchange reaction between organic iodine of Lipiodol with ionic ^{131}I was carried out with slight modifications in the reported procedure. Radioactive assay of the product was carried out using Ion chamber and yield of the product is calculated. The reaction is monitored for ^{131}I activity measurement at all the stages of production. Quality control

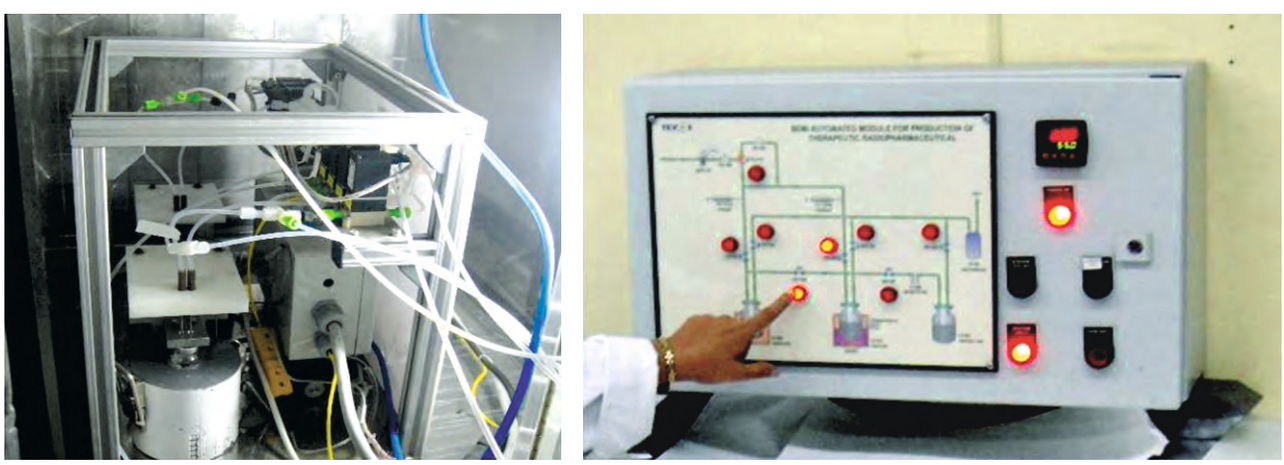

Fig. 2: Semi automated module and control panel

Table 2: Specifications of ^{131}I labeled Lipiodol and QC acceptance criteria

Product Code	IOM-40
Description	^{131}I labeled Lipiodol is ready to use sterile, pyrogen free injectable formulation. The formulation contains ^{131}I Iodinated ethyl esters of fatty acids of poppy seed oil (^{131}I labeled Lipiodol)
Appearance	Clear yellow to light brown liquid
Radionuclide identification	Principal Energy peaks 364 & 637 keV (±5keV)
Radionuclide Purity	>99.9%
Radiochemical purity	>95%
Radioactive concentration	15-20 mCi /mL
Storage	Stored between 10 to 25°C in dark with adequate shielding
Expiry	Seven days from the date of reference

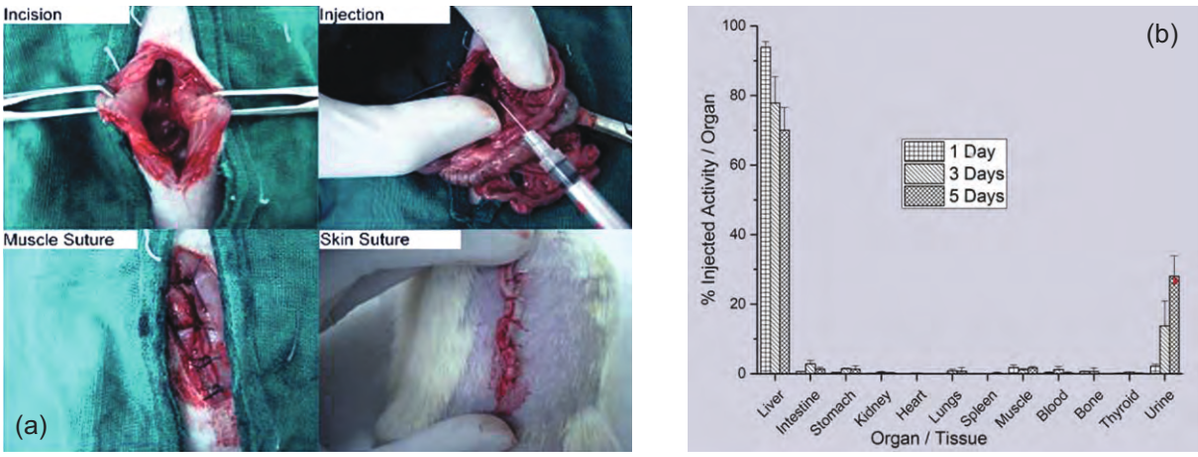

Fig 3: Preclinical evaluation in rats. (a) Procedure (b) Biodistribution data of ^{131}I-Labeled Lipiodol

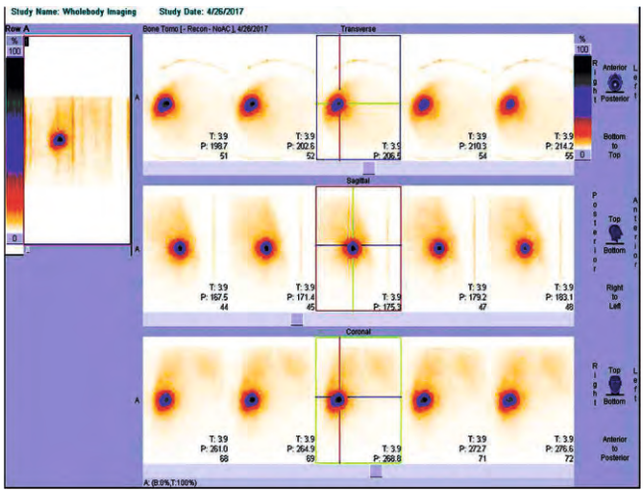

Fig. 4: Images showing the retention of activity in Liver of a patient injected with ^{131}I labeled Lipiodol

analysis by physicochemical test is done immediately after preparation for all the batches of ^{131}I labeled Lipiodol while biological tests as per Indian Pharmacopoeia are done after decay of activity. Table 2 depicts specifications of the product, ^{131}I labeled Lipiodol injection.

Pre Clinical Evalution

Animal biodistribution studies were done in normal Wistar rats using viable surgery protocol to study liver retention and kinetics over a period of 5 days post injection of ^{131}I Lipiodol. Fig 3a depicts a typical procedure used for preclinical evaluation in orthrotropic model and Fig 3b depict the biodistribution pattern confirming retention of >90% injected ^{131}I activity in liver 24h post injection.

Regulatory Approval

Dossier containing detailed production procedures, quality control monographs and data of consecutive batch production and QC was submitted and approval was obtained from DAE-Radiopharmaceutical committee on March 2017 for manufacture and supply of ^{131}I Lipiodol Injection for clinical use.

Clinical evaluation

Clinical evaluation of ^{131}I labeled Lipiodol in HCC patients started from April 2017. Production and QC of nine batches of patient dose of ^{131}I labeled Lipiodol was carried out till Dec 2017. Initial clinical results are promising with major retention of activity in liver upto 72h post injection for therapeutic response. Fig 4 depicts representative image of patient injected with ^{131}I labeled Lipiodol.

Conclusion

Radiopharmaceutical Division has successfully carried out indigenous development of therapeutic radiopharmaceutical ^{131}I labeled Lipiodol Injection and deployment of safe and pure product for clinical use as IOM-40 from BRIT (patient dose of 75mCi activity at a cost of Rs. 40,000). Initial results are very satisfying and requests from various nuclear medicine centres are being received for the product. ^{131}I labeled Lipiodol injection is a cost effective alternative for treatment of Hepatocellular carcinoma.

References:

1. Raoul JL, Boucher E, Rolland Y, Garin E et al. Treatment of hepatocellular carcinoma with intra-arterial injection of radionuclides. Nat. Rev. Gastroenterol. Hepatol 2010; 7:41–9.
2. Lambert B, Van de Wiele C. Treatment of hepatocellular carcinoma by means of radiopharmaceuticals. Eur J Nucl Med Mol Imaging 2005;32:980–89.
3. Giammarile F, Bodei L, Chiesa C, Flux G, Forrer F, Kraeber-Bodere F et.al. EANM procedure guidelines for the treatment of liver cancer and liver metastasis with intra-arterial radioactive compounds. Eur J Nucl Med Mol Imaging 2011; 38:1393-1406.
4. Ambade RN, Shinde SN. Khan MSA, Lohar SP, Vimalnath KV, Joshi PV et.al. Development of a dry distillation technology for the production of ^{131}I using medium flux reactor for radiopharmaceutical Applications. J Radioanal Nucl Chem 2015; 303:451–67
5. Mukherjee A, Subramanian S, Ambade RN, Avhad BG, Dash A, Korde A.Development of Semi-automated Module for Preparation of ^{131}I Labeled Lipiodol for Liver Cancer Therapy. Can BiotherRadiopharm 2017; 32(1): 33-7.

Indigenous Development of Adherent Nanocrystalline UO_2 Thin Films: Heart of Large Scale Fission Counters

Subir Kumar Ghosh, Jalaj Varshney and Vivekanand Kain
Materials Processing and Corrosion Engineering Division
Raghvendra Tewari
Materials Science Division
Madangopal Krishnan
Materials Group

Importance of UO_2 in the form of thin coatings is increasing significantly as various functional applications; such as target materials for fission based nuclear experiments, production of ^{99m}Tc isotope and in many other functional applications. These coatings are also used in fission counter (FC) for mapping the neutron flux inside as well as outside the core of nuclear reactors and in accelerator based Intensity-Modulated Radiation Therapy (IMRT) unit for safe operation and power regulation. However, complexity in the fabrication of uniform, adherent thin films of UO_2 on variety of shapes and substrates restricts its wide-range applicability. In this regard, a simple DC electrodeposition technique has been indigenously developed to form uniform and adherent thin coatings of UO_2 on large-scale, on variety of shapes and geometry such as circular disc, cylindrical rod and tube made of stainless steel, inconel and aluminium etc. from an alkaline uranyl-oxalate electrolyte. This work has led to the successful replacement of several imported fission counter based neutron detectors. In addition, in this process for the first time, a two-step reduction mechanism of UO_2^{2+} to UO_2 via U(V) intermediate was established in alkaline pH which provided a thin and adherent coating. Deposition process parameters were systematically optimized for the production of UO_2 thin films for large-scale fabrication of FC's. Detailed grazing incidence X-ray diffraction (GIXRD), field emission scanning electron microscope (FESEM) and high-resolution transmission electron microscope (HRTEM) investigations of the thin films revealed formation of nonporous, nanocrystalline *fcc*-UO_2 films under as-deposited condition. A suitable heat-treatment under vacuum led to improvement in the adhesion with substrates associated with grain growth. Detailed X-ray photoelectron spectroscopy (XPS) investigations confirmed stoichiometric composition of deposited UO_2 films which showed tendency towards conversion of U_3O_8 on annealing.

Keywords: Nanocrystalline UO_2, Thin films, Electrodeposition, Fission counter, FESEM, HRTEM, XPS

Introduction

Thick and thin films of UO_2 are being used to study fission based experiments for radioactive damages, reaction and corrosion products in nuclear fuel and as fission counters (FC) for the detection of neutrons. UO_2 coating based FCs are widely used to monitor neutron flux in nuclear reactors like PWR, BWR, PHWR, LWR and prototype FBR in India [1-5]. In addition, UO_2 based monitors are also being used in linear accelerators (LINACs) which, because of their improved dose distribution near patient treated area [6-7],are used for IMRT. The production of photo neutrons and neutron capture gamma rays for energies greater than 7 MeV may result in an undesired additional irradiation to the patient [8-9]. In order to avoid unwanted radiation hazard, it is essential to monitor neutron flux near the LINAC. Efforts are on to extract ^{99}Mo as fission product which produces a medical diagnostic [10] daughter product ^{99m}Tc which emits positron used in positron emission tomography (PET). However, due to radiation hazard and handling related issues, synthesis and detailed characterization of uranium oxide based films and coatings are rather limited.

In general, technical issues, such as, adhesion of film on metallic substrate and uniformity in thickness across the substrate surface are very important for the purpose of isotope production by irradiation as well as for the use in FCs. As UO_2 film in FCs experiences high temperatures, impact due to induced radiation, high vacuum and vibrations during the operation of a nuclear reactor, deposited films should have very good adhesion to withstand these external thermal, mechanical and radiation impacts. The life of a detector, in fact, depends upon its ability to adhere to the surface.

In the present study electrodeposition was used to deposit UO_2 thin films from an alkaline uranyl nitrate-oxalate complex electrolyte. Electrodeposition is a simple, cost-effective and easy to scale-up technique.

Preparation of UO_2 Thin Films

Thin films of UO_2 deposition was carried out from an electrolyte containing uranyl nitrate, ammonium oxalate ($(NH_4)_2C_2O_4$) and distilled water under DC condition. The pH of the bath was adjusted by adding dilute ammonia and maintained throughout the deposition. A constant stirring of 100 rpm was maintained during electrolysis. The substrates used were Inconel-600, SS-304, Al or polished copper and anodes used were Pt-Pd-Ru triple oxide coated Ti. Prior to electrodeposition, the substrates were cleaned in acetone followed by alkali cleaning and finally acid dip to remove residual alkali prior to dipping into actual plating bath. Deposition rate and faradic efficiency were calculated by

weighing the mass deposited on the cathode and the charge passing during electrolysis. For characterization, eelctrodeposition of UO_2 film on copper substrate was carried out at current density of 10 mA.cm^{-2}, pH of 7.5 and temperature of 80 ^{O}C. Post deposition, UO_2 coating was characterized by GIXRD to identify the crystal structure, phases and possible structural transformation during heat-treatment. The average crystallite size and microstrain at different temperatures were determined by Debye-Scherer method by analyzing the broadening of (111) XRD peak.

The surface morphology and composition of the as-deposited as well as annealed coatings were investigated under FESEM attached with energy dispersive spectroscopy (EDS). The thickness of the electrodeposited film was measured by cutting a wafer from the coated surface using focused ion beam (FIB) attached with FESEM. The adhesion of the as-deposited as well as annealed UO_2 coating was measured by alpha counting on swapped tissue paper and by tape test. Microstructural investigation of the as-deposited as well as annealed films was done under HRTEM (JEOL 3010). XPS spectra were recorded from the top surface of as-deposited as well as annealed films for confirmation of oxidation states.

Results and discussions

CV analysis

Figure 1 shows the cyclic voltammograms of the electrolyte containing U(VI) species recorded in the potential range -0.9V to +0.5V at different scan rates in the range 50-200 mVs^{-1} (Fig.1). In the cathodic region, a very weak reduction peak at -0.076V *vs.* saturated calomel electrode (SCE) and a strong peak at -0.58V *vs.* SCE were identified. Similarly, in the anodic region, the corresponding oxidation peaks for c_1 and c_2

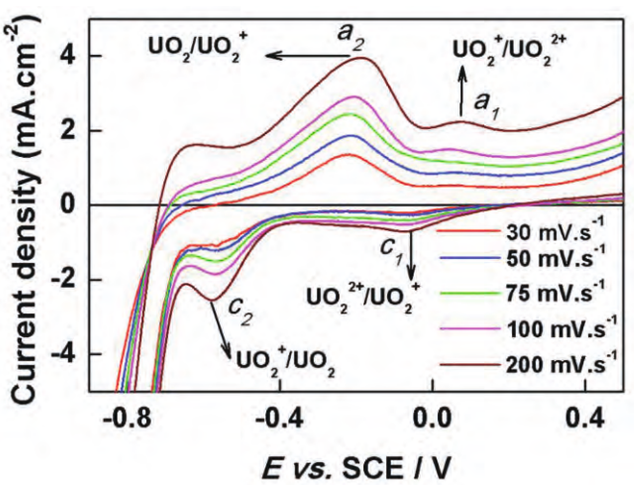

Fig.1: CV diagram of 2.5 mM $UO_2(NO_3)_2$ + 0.2M $(NH_4)_2C_2O_4$ electrolytes after passing 500^{O}C charge at different scan rates from 30 to 200 mV.s^{-1} at pH 7.5 and 80 ^{O}C.

appeared at +0.018 and -0.48 V *vs.* SCE are designated as a_1 and a_2 respectively. A strong anodic peak at -0.69 V *vs.* SCE corresponds to re-oxidation of evolved hydrogen at the fresh or uncovered Pt electrode. A large asymmetry between the cathodic and anodic peaks is also an indication of difference in the barriers to electron transfer in the forward and backward reactions that reflects in the value of charge transfer coefficient. Here, the redox peak pair c_1/a_1 is identified as UO_2^{2+}/UO_2^+ couple and the pair c_2/a_2 is identified as UO_2^+/UO_2 couple. Therefore, it is confirmed that the reduction of UO_2^{2+} to UO_2 is a two step process for which the first step UO_2^{2+} to UO_2^+ is quasi-reversible in nature and is a rate determining step. For a quasi-reversible diffusion controlled electrochemical reaction, the peak current (i_{pc}) is related to the scan rate by Delahay [11] equation as follows.

$$i_{pc}=0.4961(RT)^{-1/2}F^{3/2}n^{3/2}a^{1/2}CAD^{1/2}v^{1/2} \quad (1)$$

Here R is universal gas constant (8.314 J K^{-1} mol^{-1}), T is the temperature of electrolyte in K, F is Faraday constant 96487 C, n is number of electrons transferred, C is the concentration of electrolyte in mol cm^{-3}; A is the area of electrode 0.5 cm^2; D is diffusion coefficient in cm^2 s^{-1}, v is scan rate in V s^{-1} and α is charge transfer coefficient. A linear relationship between the peak current density, i_{pc} and the scan rate, $v^{1/2}$, was obtained which suggests diffusion controlled mass transport of uranyl species to the electrode surface. Assuming n = 1, the average diffusion coefficients of UO_2^{2+} and UO_2^+ complex species in the aged electrolyte estimated were 7.034× 10^{-6}cm^2.s^{-1} and 1.412× 10^{-4}cm^2.s^{-1} respectively at 80^{O}C.

In the studied pH range 5.5-8.5, a comprehensive speciation calculation using MinteqA2 software revealed the order of abundance of various species in the electrolyte: $[UO_2(C_2O_4)_3]^{4-}$ (ML_3 where M = UO_2^{2+} and L = $C_2O_4^{2-}$) >> M_2L_5 > ML_2 >> M_2L_3≈ML. Based on the electrochemical observation and speciation present the overall reduction can be described as [12]:

Step.1 Simple one electron reduction step at (-0.076 V *vs* SCE)

$$[UO_2(C_2O_4)_3]^{4-} + 1e^- \rightarrow [UO_2(C_2O_4)_3]^{5-} \quad (2)$$

Step.2 Proton assisted one electron reduction at (-0.58 V vs SCE)

$$[UO_2(C_2O_4)_3]^{5-} + H^+ + 1e^- \rightarrow [HUO_2(C_2O_4)_3]^{5-} \quad (3)$$

Later this intermediate complex species undergoes alkaline hydrolysis to form UO_2 (s)

$$[HUO_2(C_2O_4)_3]^{5-} + OH^- \rightarrow UO_2\,(s) + H_2O + 3C_2O_4^{2-} \quad (4)$$

Based on existing predominant ML_3 species in an alkaline media, for the first time a detailed electrochemical reduction mechanism of uranyl ions is elucidated.

Effect of current density on deposition rate

In order to study the variation of deposition rate and current efficiency, the current density was varied in the range of 5-50 mA.cm^{-2} by keeping temperature and pH constant at 80^{O}C and 7.5 respectively. With increase in current density, an increasing trend of deposition rate upto 30 mAcm^{-2} was visible (Fig. 2) which subsequently reduced upon increasing current density beyond 30 mA.cm^{-2}. The maximum deposition rate of 4 mg.cm^{-2}.h^{-1} was achieved at 30 mA.cm^{-2}.

On the contrary, the current efficiency of deposition was found to decrease monotonously with increasing current density; e.g. 9% at 5 mA.cm^{-2} to 2% at 50 mA.cm^{-2}. This indicates that the cathodic reduction is favorable at low current density region. The coverage on cathode surface was uniform and black in color throughout the studied current density range.

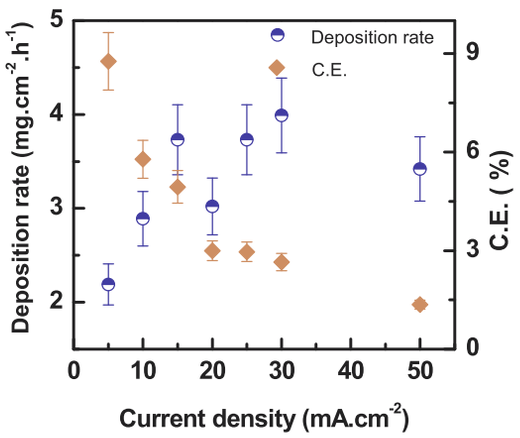

Fig. 2: Effect of current density on deposition rate and current efficiency of UO_2 deposition at constant temperature T= 80 ^{o}C and pH = 7.5.

Effect of pH on deposition rate

Figure 3 shows that with increase in pH of the electrolyte, the deposition rate of the UO_2 coating increased. Upon increasing pH to 9.0, the rate of the deposition decreased due to partial precipitation of the ammonium di-uranate. It is also clear that for the identical variation of pH the faradic efficiency of deposition enhanced commensurately with the deposition rate. The overall current efficiency (CE) was between ~2 to 9%. In the present study, a maximum current efficiency obtained was 8.5% at pH 8.75. Like deposition rate, the CE was also found to decrease at pH 9.0. Between pH 7.0-7.5, the overall surface was mat-black; it turned into shiny black between pH 7.75-8.25, and again back to mat-black finish from pH 8.5 onwards. Therefore, the pH range 7.5-8.5 was chosen as the optimized range for the deposition of UO_2 from this electrolyte.

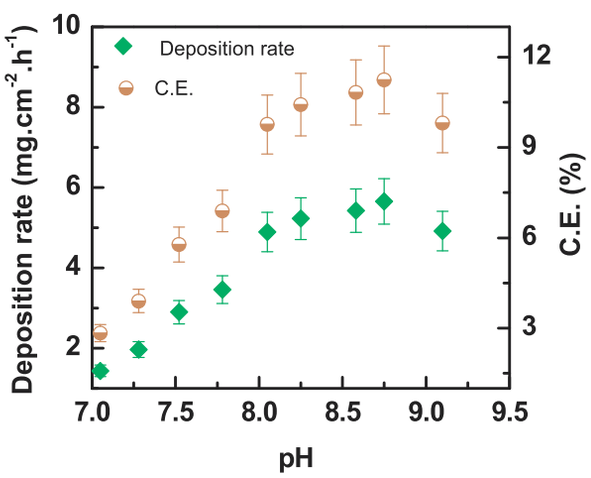

Fig. 3: Effect of pH on deposition rate and current efficiency of UO_2 deposition at constant c.d. of 10 mA.cm^{-2} and T = 80 ^{o}C.

Effect of temperature on deposition rate

Figure 4 shows that with increase in temperature of the electrolyte, the deposition rate and current efficiency increased. At 60 ^{o}C, the deposition rate was 0.75 mg.cm^{-2}.h^{-1} which increased to 3.5 mg.cm^{-2}.h^{-1} at 85 ^{o}C. Therefore, a five-fold increase in deposition rate was recorded for a change in temperature of 25 ^{o}C indicating significant influence of electrolyte temperature on deposition rate. Similarly, the CE of deposition was also increased from 1.5% at 60 ^{o}C to 5.5% at 85 ^{o}C.

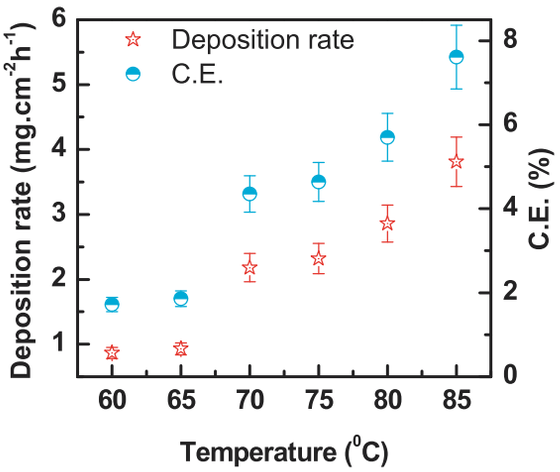

Fig. 4 Effect of temperature on deposition rate and current efficiency of UO_2 deposition at constant c.d. of 10 mA.cm^{-2} and pH = 7.5.

Figure 5 shows typical UO_2 coated Inconel-600 discs in as-deposited as well as after annealed conditions. A uniform adherent black color UO_2 layer is visible on Inconel-600 surface under as-deposited condition which was converted into greyish in color upon annealing at 700 ^{o}C for 1 h. The adhesion of deposited coating was checked by swapping white tissue paper and found that nearly all coatings were adherent to the substrate. No significant black color particles were visible on the tissue paper. The coating adhesion was also checked by sticking adhesive scotch tape and found no visible black particles on it after taking out from the coating surface. In addition, alpha particle counter showed considerably low counting on the tissue papers swapped through the annealed UO_2 coated samples (20±5 counts per minutes) in comparison

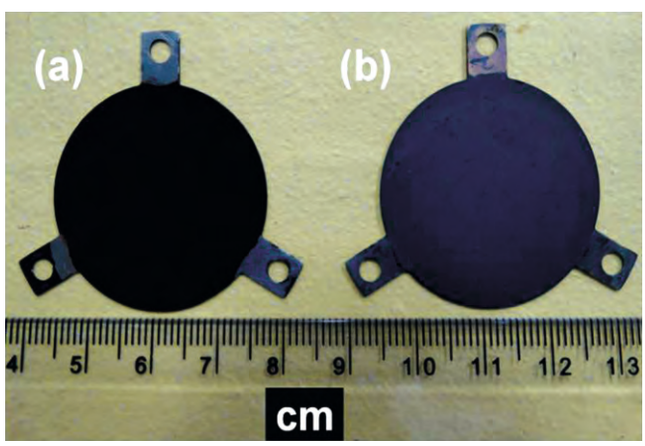

Fig. 5: Optical micrographs of UO_2 coating on inconel-600 substrate under (a) as-deposited and (b) annealed conditions at 700 ^{o}C for 1 h.

to as-deposited samples (35±5 counts per minutes). This indicates that the adhesion of the coating was improved significantly upon annealing under vacuum. Such improved adhesion of annealed samples could be attributed to the formation of spinel structure between UO_2-CuO interface.

Crystal Structure and phase analysis

Grazing incidence XRD patterns recorded on UO_2 coatings starting from as-deposited to stepwise vacuum annealed samples up to 700 ^{o}C are shown in Fig. 6. As-deposited sample shows a broad peak at 28.16^{o} indicating amorphous or ultra-nanocrystalline structure of the coating. Upon annealing, a systematic increase in intensity of peak at 28.16^{o} is observed along with appearance of several broad small intensity peaks at 35.28^{o}, 46.86^{o} and 55.62^{o} from the sample heated up to 500 ^{o}C. This indicates about the absence of large crystallites of UO_2 under as-deposited condition but upon annealing, a tendency to form large polycrystalline crystal structure increases. Such transformation is an indication of the start of crystallization process. At even higher temperature 600^{o}C, these reflections become sharper and intense revealing an increased crystallite size. At 700 ^{o}C, the peaks corresponding to 28.16^{o}, 32.58^{o}, 46.86^{o}, 55.62^{o}, 58.33^{o}, 68.52^{o}, 75.67^{o}, 78.09^{o}, 87.15^{o} matched well with (111), (200), (220), (311), (222), (422), (331), (420) (422) reflections of *fcc* UO_2 crystal structure (PCPDF no. 780725). The emergence of high intensity (111) peak, which is much higher than the peaks obtained in a random XRD pattern of UO_2 structure, indicates the appearance of a texture in the thin films formed with {111} planes parallel to the film surface, i.e., (111). Detailed (111) peak broadening analysis between 27 ^{o}C and 700 ^{o}C revealed increase in the average grain size and commensurate decrease in micro-strain of the UO_2 coating with rise in annealing temperature [13]. The average grain size is less than 2 nm at 27 ^{o}C, and becomes 5.8 nm at 600 ^{o}C. Beyond 600 ^{o}C, there occurs a rapid grain growth and ultimately it becomes 13.2 nm at 700^{o}C.

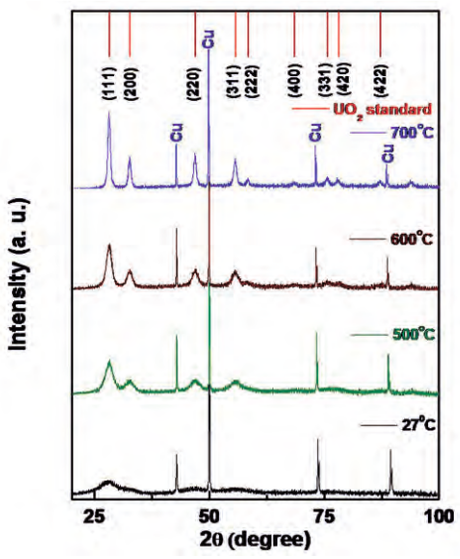

Fig.6 XRD-patterns of UO_2 coating at different temperatures recorded during stepwise annealing. UO_2 standard lines are form PCPDF no. 780725 file.

Surface morphology

Surface morphology of as-deposited UO_2 coating showed typical nodular growth pattern containing shallow cracks on the surface as shown in Fig. 7(a). The composition analysis of as-deposited coating showed a U:O of 1:5. This higher oxygen content in the coating could be attributed to the oxidation of deposited uranium oxide coating in the presence of air. Post annealing showed appearance of through thickness network of cracks in the coating, as shown in Fig. 7(b). The formation of such network of cracks is attributed to partial lateral shrinkage of coating because of crystallization from voluminous amorphous phase and evaporation of adsorbed water molecules at higher temperature (700 ^{o}C). It is also evident that the annealed coating contains lot of pores. In order to ascertain possibility of complete exposure of substrate, EDS was taken both from the plateau region of coating surface as well as from the crack region. EDS results from cracked region clearly showed that U and O-content are comparatively lower in comparison to Cu indicating larger penetration of incident electron beam. It confirms that in the cracked region a thin layer of UO_2 still exists on the Cu-substrate. Similarly, higher U and O-content from plateau region of the coating along with lower Cu content describes a fairly lower extent of penetration of incident electron beam into the Cu-substrate after crossing the thickness of UO_2 coating. We also note that the composition analysis from

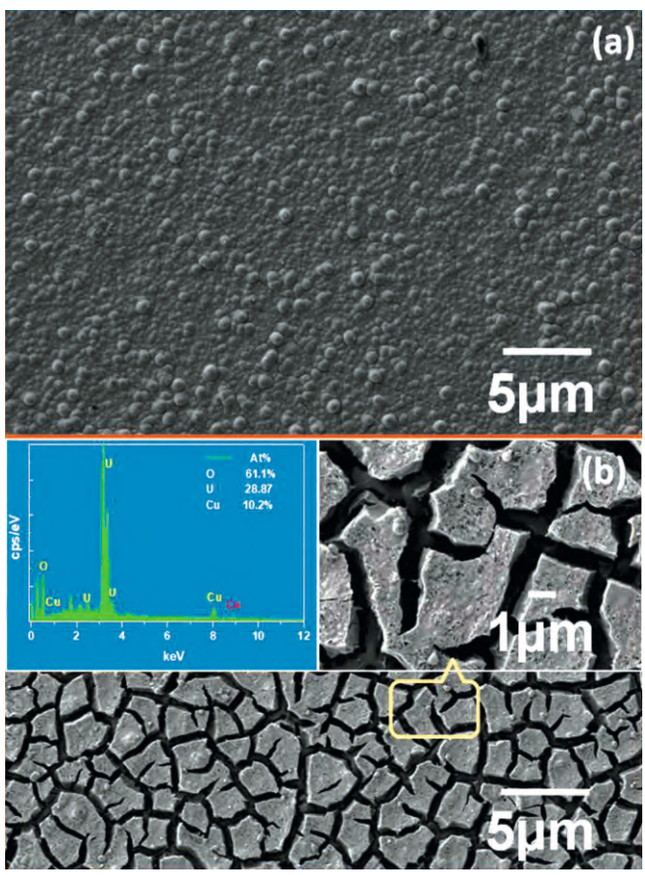

Fig. 7 (a) FESEM micrograph of as-deposited UO_2 surface; (b) annealed (700 ^{o}C for 1 h) UO_2 surface; Inset shows magnified image of the annealed surface showing opened up cracks and pores and EDS spectrum showing presence of U, O and Cu as base substrate.

coatings plateau as well as cracked region shows U:O1:2. This result proves that even after crack formation the surface of the substrate is not fully exposed rather a very thin layer of UO_2 still exists.

Cross-section morphology of the as-deposited coating was investigated to reveal the UO_2 coating thickness and UO_2-Cu interface structure [13]. Examination of typical cross section image of the UO_2 coated Cu substrate showed that the coating formed on the substrate surface is nearly uniform in thickness. The coating thickness measured as ~6 μm. A clear gap between the oxide coating and the metal surface was observed indicating poor adhesion. In this case, basically the mechanical entangles between coating and substrate contours are responsible for the adherence of the coating. No porosity in the coating lamella was visible even though presence of cracks was very evident. The presence of minute amount of Cu on UO_2 and U on Cu side was attributed to migration of elements during FIB ion milling.

On the other hand, cross-section micrograph of the annealed sample (Fig. 8) shows presence of large numbers of pores within the coating and clear bonding between UO_2 and Cu-substrate at certain points. It is also evident that the pores are interconnected or isolated with typical sizes ranging from nanometer to micrometers. The measured thickness of annealed sample is ~7 μm which is nearly same as as-deposited coating. The formation of large number of pores is attributed to spontaneous evaporation of adsorbed moisture and hydrogen gas during crystallization of amorphous oxide coating. Fig.8 shows typical elemental mapping across UO_2-Cu interface corroborating XRD results.

XPS analysis of UO_2 film

Figure 9 (a) shows experimental XPS curve along with deconvoluted and full fitting spectra of as-deposited UO_2 film. Two main peaks appeared at binding energies of 381.1 eV and 391.9 eV corresponding to U $4f_{7/2}$ and U $4f_{5/2}$ respectively which are referenced to C1s at 285 eV. The separation between U $4f_{7/2}$ and U $4f_{5/2}$ due to spin-orbital interactions is 10.8 eV corroborating the previous reported results [14]. Similarly, the separation between binding energies of U^{4+} (380.5 eV) and U^{6+} (381.9 eV) components of U $4f_{7/2}$ is 1.4 eV again supporting

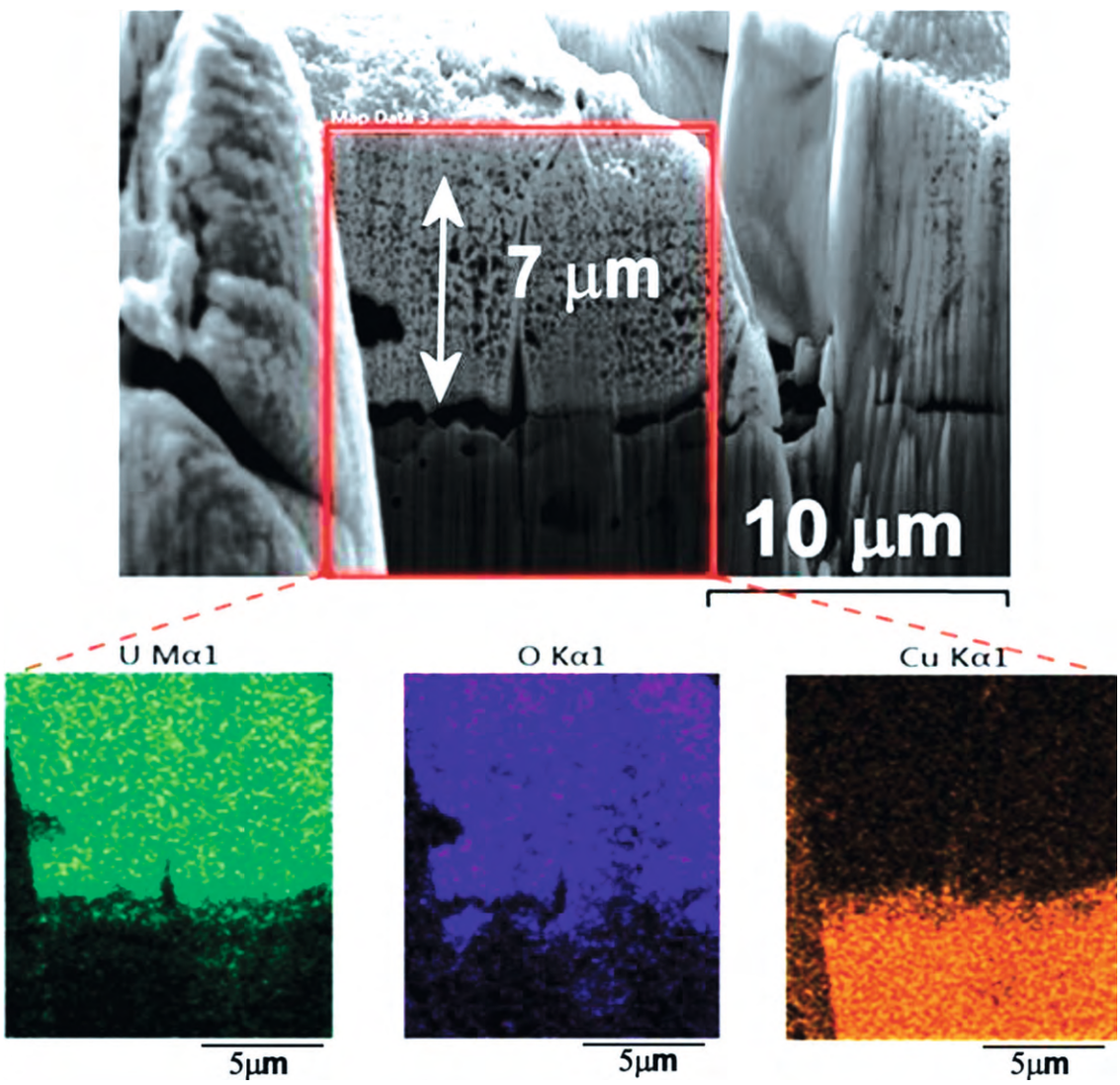

Fig.8 FIB cut cross-section FESEM image of annealed (700 °C for 1 h) UO_2 coating showing thickness and microstructure of the coating and coating-substrate interface; (b) elemental distribution of U, O and Cu across the coating-substrate interface.

the reported data [14-17]. The presence of two different oxidation state of uranium was further ascertained by the appearance of two satellites adjacent to the main peaks. For example, the positions of satellites for U $4f_{7/2}$ peak were 385.3 and 387.4 eV corresponding to U^{6+} and U^{4+} components. It is also noted that the intensity of U^{4+} component is relatively higher in comparison to U^{6+} component in both U $4f_{7/2}$ and U $4f_{5/2}$ peaks which confirms about the formation of UO_2 as primary species in as-deposited state supporting the high temperature XRD results. A relatively low intensity of U^{6+} state (UO_3) attributes to partial aerial oxidation of surface layers of as-deposited UO_2. In fact, UO_2 has inherent tendency to oxidise into different forms of oxides depending upon temperature and morphology [18-19].

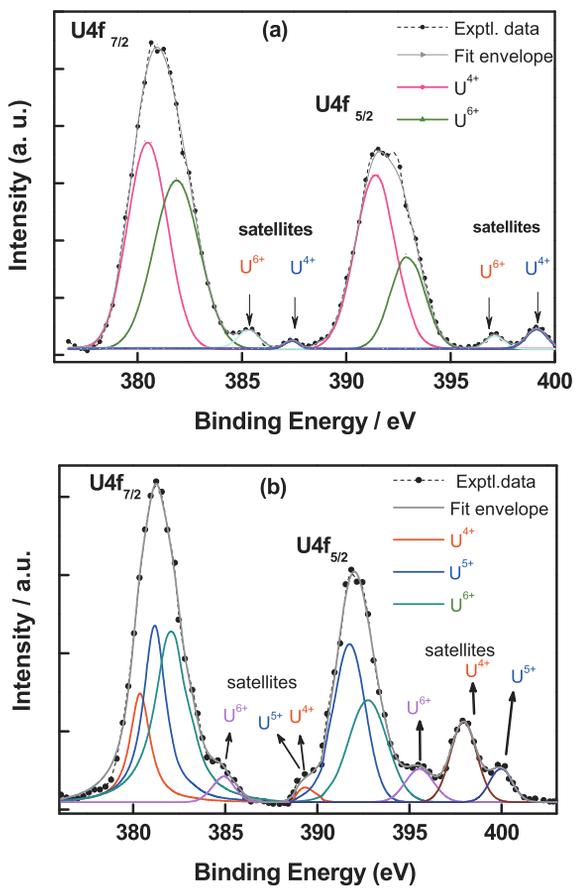

Fig. 9: U4f XPS spectra of (a) as-deposited and (b) annealed (700 °C for 1 h) UO_2 films.

Figure 9(b) shows experimental and full spectrum fitting along with satellites of U 4f XPS spectra of annealed UO_2 coating. Unlike as-deposited surface, the presence of U^{5+} along with U^{4+} and U^{6+} were identified along with their satellites. The main peaks correspond to U $4f_{7/2}$ and U $4f_{5/2}$ appeared at binding energies of 381.4 and 392.1eV. Similarly, all three deconvoluted components of U^{4+}, U^{5+}, and U^{6+} of U $4f_{7/2}$ peak have appeared at binding energy values of 380.4 eV, 381.1 eV and 382.0 eV respectively. These binding energies and the separation between the component peaks are estimated to be 1.6, 0.9, and 0.75 eV for U^{6+}- U^{4+}, U^{6+}- U^{5+} and U^{5+}- U^{4+} respectively supporting the reported results [15,20] on presence of mixed oxides of uranium. It is noted that the satellite of U^{6+} component in U $4f_{7/2}$ spectrum has appeared at 384.9 eV, however, the satellite peaks for other two components (U^{5+} and U^{4+}) are basically submerged within the main U^{4+}component of U $4f_{5/2}$ spectrum [14] which are indicated in the Figure 9(b). However, all the three satellites corresponding to U^{6+}, U^{5+} and U^{4+} components of U $4f_{5/2}$ spectrum are clearly visible at 395.5 eV, 399.9 eV, and 397.9 eV respectively. However, the satellite that appears at 399.9 eV corresponds to the mixed valence state of U^{6+}& U^{5+} [16]. Detailed analysis of the fitted spectrum showed the relative order of intensities as U^{6+}> U^{5+}> U^{4+} indicating temperature induced oxidation of UO_2 to UO_3 via mixed valence oxides in the presence of trace amount of oxygen [18-19]. These results are in accordance with the XRD results of air-annealed UO_2 coatings [13].

HRTEM of UO_2 film

Figure 10(a) shows the distribution of the UO_2 particles in the as deposited sample. SAD pattern obtained from one such cluster is shown in Fig.10(b). Typical ring pattern confirms the nano-size particles distributed within the cluster. Based on the ratio of the radii of rings, each ring was successfully indexed in terms of *fcc* UO_2 phase. Detailed investigation of the microstructure showed that most of the crystallites were below 5 nm. Fig.10 (c) shows particle distribution in the sample. From the distribution graph it can be noticed that majority of the particles are in the range of 1-4 nm. The

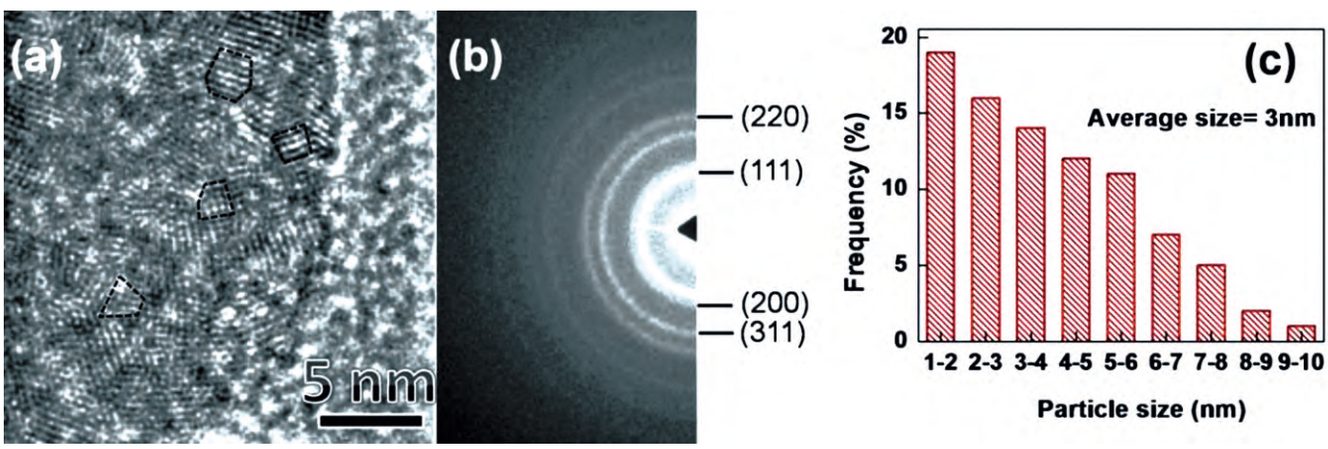

Fig. 10: (a) HR-TEM micrograph of as-deposited UO_2 coating showing several nano crystallites (outlined) and their distribution; (b) SAED pattern of as deposited UO_2 coating and (c) UO_2 particle size distribution in as-deposited film.

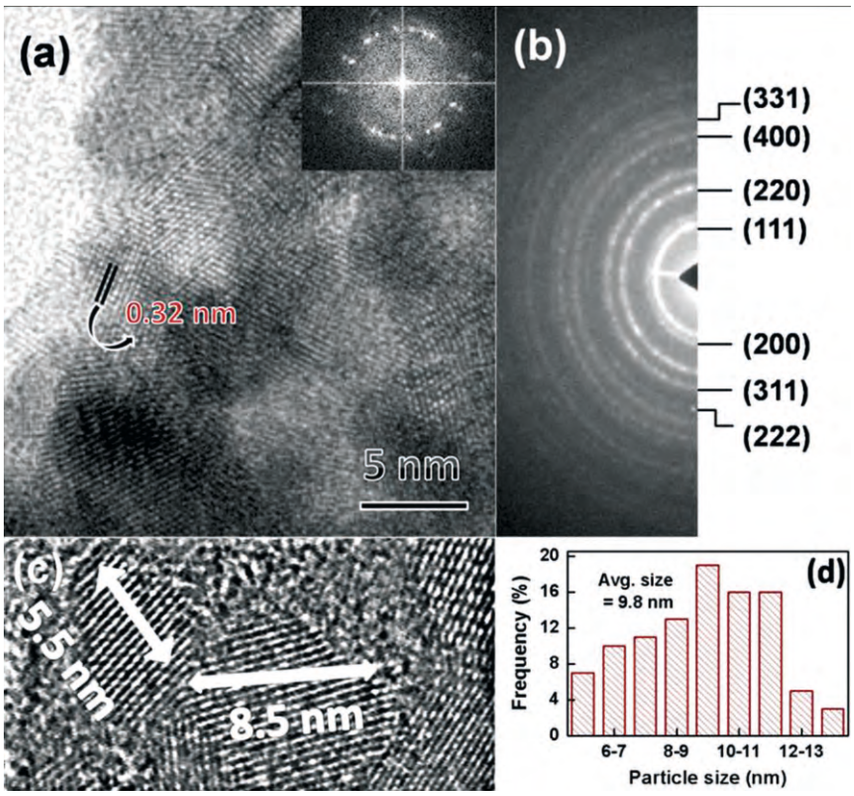

Fig. 11: (a) HR-TEM micrograph of annealed UO_2 coating showing distribution of crystallites, inset showing FFT pattern from the same image; (b) SAED pattern of annealed UO_2 coating (c) high magnification image showing grain growth and gain morphology; (d) UO_2 particle size distribution in annealed (700 ^{o}C for 1 h) film.

estimated average particle size was 3.0 nm. Fig. 11(a) shows the distribution of the UO_2 particles in the annealed samples. In annealed sample, it may be noticed that the crystallites become well defined and the average size of the crystallites has increased. Fast Fourier Transformation (FFT) of the image is shown as inset in Fig. 11 (a). Distinct reflections and well separation between the particles clearly indicate that particles are nearly strain free and in well-annealed condition. Increase in the particle size is further corroborated from the differences in the ring patterns of the two SAD patterns. SAD pattern from the annealed sample showed discrete nature of the rings (Fig.11(b)) which is in contrast to the continuous rings observed in the case of as-deposited samples. Fig. 11 (c) shows the magnified view of few such crystallites. Distinct planar arrangements of lattice helped in clearly identifying the crystallite of UO_2. Fig. 11 (d) shows particle distribution in the annealed sample. From the distribution graph it can be seen that majority of the particles are in the range of 8-12 nm. The average particle size was estimated as 9.8 nm. This clearly shows that during annealing not only the particles attained well define structure but coarsened also.

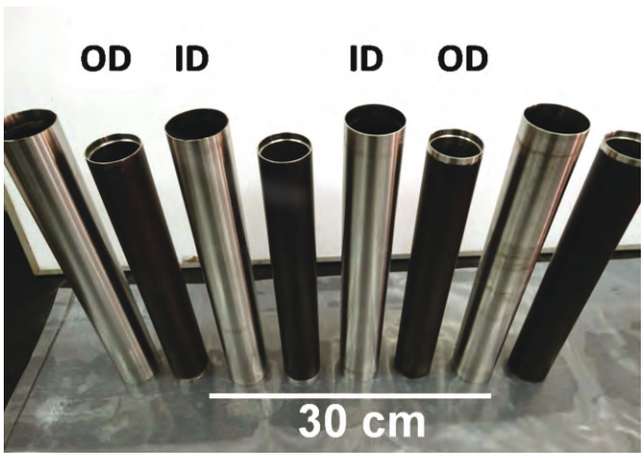

Fig. 12: Uniform adherent UO_2 thin film coated (ID as well as OD) stainless steel tubes.

In short, the current method of using alkaline uranyl-oxalate complex electrolyte to produce adherent nanocrystalline UO_2 coating of ~6-7 μm thickness has been successfully developed and high reproducibility of large scale uniform coating has been demonstrated. Fig.12 shows typical examples of tubes where in regular ways UO_2 coatings on the inner or outer surface or on both the surfaces of tubes are produced.

Conclusions

In the present study, smooth, adherent nanocrystalline UO_2 coating of ~6-7 μm thickness was successfully electrodeposited by simple DC electrolysis from an alkaline uranyl-oxalate complex electrolyte. For large scale deposition, the parameters were optimized for obtaining adherent coating as; current density of 10-25 mA.cm^{-2}, pH = 7.5 to 8.5 and temperature of 80±2 ^{o}C. Surface morphology of as-deposited coating showed smooth deposition with fine nodules and cracks. Post annealing cracks were widened on the surface of UO_2 film but with improved adhesion with substrate. XRD analysis of the as-deposited coating showed amorphous nature of the coating which turned into nanocrystalline *fcc* UO_2 upon vacuum annealing to 700 ^{o}C. Cross-section FESEM revealed highly porous nature of annealed UO_2 film. Detailed GIXRD, HRTEM and EDS composition analyses confirmed that the deposited coating was having O/U ratio as 2:1. HRTEM investigation clearly showed the formation of ultra-nanocrystalline UO_2 films with majority of the particles in the range of 1-4 nm. Upon annealing at 700 ^{o}C for 1 h, a clear grain growth was noticed due to association of smaller crystallites into a bigger one with particle size in the range 8-12 nm. XPS analysis confirmed the formation of UO_2 in as-deposited condition with a small percentage of UO_3 formed on the top surface layer due to aerial oxidation. In annealed sample, the presence of mixed valence oxides was more prominent due to oxidation in the presence of adsorbed water and oxygen into the films. A clear two-step mechanism of UO_2 film deposition in alkaline medium was successfully demonstrated.

Acknowledgements

The present work was not possible without the support of Electronic Division, BARC. Authors greatly acknowledge the unconditional support and constant encouragement by Dr. D. Das, Associate Director, E&IG Group and Dr. A. Behere, Head, Electronics Division.

References

1. Crane, T.W. and Baker, M.P., *Neutron detectors." In Passive Nondestructive Assay of Nuclear Materials* ed. by D. Reilly et al., Nuclear Regulatory Commission, *NUREG/CR-5550*, 1991, 379-406.
2. Ambrosi, P., Radiation protection and environmental standards. Metrologia, 2009, 46(2), S99-S111.
3. Shao, Q., Radev, R.P., Conway, A.M., Voss, L.F., Wang T.F., and Nikolic, R.J., *SPIE Defense, Security, and Sensing. Radiological and Nuclear detection*, 2012, 8358-8360.
4. Sivaramakrishna, M., Nagaraj, C.P., Madhusoodanan, K., and Chellapandi, P., Neutron Flux Monitoring System in Prototype Fast Breeder Reactor. *Int. J. Eng. Innovative Technol.*, 2014, 3, 45-53.
5. Vijayakumaran, P.M., Nagaraj, C.P., Paramasivan Pillai, C., Ramakrishnan, R., and Sivaramakrishna, M., *Nuclear Instrumentation Systems in Prototype Fast Breeder Reactor,* Paper No. ICONE12-49354, pp. 457-463; *12th International Conference on Nuclear Engineering*, Volume 2, Arlington, Virginia, USA, April 25–29, 2004.
6. Martínez, S. A., Barquero, R., Gómez-Ros, J. M., Lallena, A. M., Andrés, C., and Tortosa, R., Evaluation of neutron production in new accelerator for radiotheraphy. *Radiat. Measure.*, 2010, 45, 1402-1405.
7. Golnik, N., Zielczynski, M., Bulski, W., Tulik P., and Palko, T., Measurements of the neutron dose near a 15 MV medical linear accelerator. *Radiat. Prot. Dosim.*, 2007, 126, 619-622.
8. Followill, D.S., Stovall, M.S., Kry S.F., and Ibbott, G.S., Neutron source strength measurements for Varian, Siemens, Elekta, and General Electric linear accelerators. *J. Appl. Clinical Med. Phys.*, 2003, 4, 189-194.
9. Nedaie, H.A., Darestani, H., Banaee, N., Shagholi, N., Mohammadi, K., Shahvar A., and Bayat, E., Neutron dose measurements of Varian and Elekta linacs by TLD600 and TLD700 dosimeters and comparison with MCNP calculations. *J. Med. Phys.*, 2014, 39, 10-17.
10. Saliba-Silva, A.M., Garcia, R.H.L., Bertin, E., de Carvalho, E.F.U., and Durazzo, M., Uranium electrodeposition for irradiation targets. *ECS Trans.*, 2013, 45 (9), 5-12.
11. Delahay, P., New Instrumental Methods in Electrochemistry: Theory, Instrumentation, and Application to Analytical and Physical Chemistry, Interscience, New York, 1954.
12. Rajak, S., Ghosh, S.K., Varsheny, J., Srivastava, A., Tewari, R., Kain, V., 2018. Electrochemical investigation of uranyl species reduction in alkaline oxalate electrolyte and microstructural characterization of deposited nanocrystalline UO_2 thin films. *J. Eelctroanl. Chem.* 2018, 812, 45-53.
13. Varshney, J. Rajak, S. Ghosh, S.K. Vishwanadh, B. Tewari, R. Kain, V. and Dey, G.K., 2016. Electrosynthesis and Characterization of Nanocrystalline UO_2 Coating from Aqueous Alkaline Electrolyte. *RSC. Adv.* 2016, 6, 112646-112655.
14. Bera, S., Sali, S. K., Sampath, S., Narasimhan, S.V., Venugopal, V., Oxidation state of uranium: an XPS study of alkali and alkaline earth urinates, *J. Nucl. Mater.* 255 (1998) 26-33.
15. Ilton, E.S., Haiduc, A., Cahill, C.L., Felmy, A.R., Mica surfaces stabilized pentavalent uranium, *Inorg. Chem.* 44 (2005) 2986-2988.
16. Van den Berghe, S., Laval, J.-P., Gaudreau, B., Terryn, H., Verwerft, M., XPS investigations on cesium uranates: mixed valency behaviour of uranium, *J. Nucl. Mater.* 277 (2000) 28-36.
17. Hedhili, M.N., Yakshinskiy, B.V., Madey, T.E., Interaction of water vapor with UO_2 (001), *Surf. Sci.* 445 (2000) 512-525.
18. McEarchern, R. J., Taylor, P., A review of the oxidation of uranium dioxide at temperatures below 400°C, *J. Nucl. Mater.* 254 (1998) 87-121.
19. Idriss, H., Surface Reactions of Uranium oxide powder, thin films and single crystals, *Surf. Sci. Rep.* 65 (2010) 67-109.
20. Finnie, K.S., Zhang, Z., Vance, E.R., Carter, M.L., Examination of U valence states in the brannerite structure by near-infrared diffuse reflectance and X-ray photoelectron spectroscopies, *J. Nucl. Mater.* 317 (2003) 46-53.

Criticality Evacuation Management System in Fissile Material Handling Laboratories of Radio-Metallurgy Facility of BARC

Manisankar Dhabal, P. Nagaraju and Ashok Kumar
Hot Lab Utility & Engineering Services Section
Narendra Kumar Karnani
Engineering Design & Development Division

Abstract

A potential criticality risk hazard exists when large quantities of fissile materials are handled in nuclear facilities. The most important aspect of criticality safety is accident prevention because of the potentially serious consequences that can result. Based on criticality analysis various methodologies are adopted to control criticality in such facilities. In spite of effective criticality control methods put in place there lies a chance of criticality emergency and hence such facilities need criticality detection and evacuation system to minimise the personal exposure in such emergency. Establishing an effective evacuation management system is also an equally important safety requirement for prompt evacuation from the facility. The criticality evacuation management system has been designed, implemented and commissioned in an important facility at Trombay. This technique has saved laying large nos. of cables and improved the reliability of annunciation system by using state of art latest components. It has self-diagnosis facility, which is very helpful for prompt diagnosis and immediate replacement in case of malfunctioning.

Keywords: RMD, Criticality, Ionization Chamber, Ethernet, DIO

Introduction

To prevent and detect criticality accident is most important aspect in Radiological laboratories where fissile materials are being handled. When a critical mass or volume (depends on a number of factors i.e. size, shape and composition) of fissile material comes together then criticality may arise. This refers to a stage when self-sustaining or uncontrolled neutron chain reaction occurs.

The plant should be inherently safe against criticality and should haveactive engineered practices such as various detection instruments, material movement control hardware etc. Strict administrative safety measures are followed after extensive study of criticality risk assessment. Most common methodology for criticality is by control of mass. About 0.5 kg of plutonium 239 or 48 kg of uranium in certain geometrical configuration may lead to criticality [1]. As per IRSN report about 60 criticality accidents have occurred worldwide since 1945 and most of them are in research reactor or critical assemblies [2] Report says approximately 45% reported accidents occurred in 2011-12 are in case of criticality control by mass of fissile material [1]. Priority is always given to prevent criticality accidents. In spite of having all measures to control handling and storage of fissile materials there always remains a risk of failure of administrative and active control or an unprecedented event which may give rise to criticality accident. In a large radioactive facility there are significant numbers of occupational workers and consequently criticality may give rise to exposure of persons or spread of radioactivity within the facility. It requires an emergency response arrangement along with early detection of criticality and an alarm system for the evacuation as promptly as possible. Study on criticality detection system has been done and it has been found that criticality detection is possible only after the chain reaction is initiated (Details of detection instrument is given in subsequent section). Hence it is not possible to prevent exposure to nearby operator where the criticality has initiated. However in a large plant where there are significant no. of occupational workers working inside the same facility at other radioactive laboratories or at nearby sitting rooms, it will take some time to spread the radioactivity to the whole area. By this time all these occupational workers have to be evacuated from the facility. Radiological consequences of criticality can be minimised provided a prompt evacuation from the facility can be arranged. This would require a system which will automatically guide all the workers to come out from the facility in a time as low as reasonably possible. This paper describes design and establishment of an intelligent evacuation management system to manage criticality accident condition in an existing facility. The system is easy for implementation and has provisions for periodical testing and continuous monitoring of functionality of the components. The system has been successfully implemented, commissioned in RLG Radio metallurgy Wing.

Methodology

In order to design an evacuation system following basic data for the facility is considered. These are (a) No. of persons working in the facility, (b) Location of dedicated Radio-Health Physics Unit, (c) Entry and exit points of the facility, (d)Geographical distribution of active laboratories susceptible to criticality risk hazard, (e) Availability and location of control

room and/or security post which is 24 hours manned and (f) Availability and location of emergency exits.

Based on the functionality requirements, various components required for the overall system are a) Criticality Detection System, b) Audio Visual Annunciation System , c)Controller for the Annunciation system&d)Exit Indicators.

While selecting the components following criteria has been followed:

a) Maximum distance of the annunciation system from the farthest worker
b) Easy Connectivity between various components
c) Simple method for Periodical Testing
d) Online status of components used
e) Authorized Access to the control system
f) Availability of Components
g) Location of the components to be mounted

A scheme has been designed for RMD facility inside RLG, BARC. Components have been selected based on the scheme given in Fig 2.

Description of the facility

Radio-Metallurgy facility is located inside RLG, BARC Trombay. The Radio metallurgy Wing is provided with once through laboratory ventilation. Fume hood, glove boxes are provided for radioactive material handling. Glove boxes are located in the laboratories and a common glove box exhaust ventilation system is provided for it. Main laboratories are provided with both supply and exhaust air ventilation system. Glove boxes are provided separate exhaust ventilation system with no supply. There is a dedicated Radio-health physics unit (RHC) for the facility. RHC unit keeps record of the personnel monitoring through TLD, monitors area monitors located at various wings.

Detection System

The laboratories are equipped with Criticality Alarm Systems by detecting gamma radiation. In a criticality event there is always an initial spike of Gamma radiation dose rate which exceed by three decades from background with in a time of 0.2 mili second to 3 seconds and even a smallest criticality will give rise of gamma radiation dose rate of 3.6R/Hr at the distance of 30 meter. The IAEA Technical Committee agreed with the ISO standard and held that a gamma dose rate detector which will alarm at 0.026 mGy in250 msec. and in a steady field of 36 mGy/h is adequate to detect a criticality excursion of 10^{15} fissions at 30 meters away[4].

System Description:

Criticality Alarm System is based on the ISO standard and is designed to give alarm at the threshold as mentioned above. It consists of three criticality monitors and a system criticality alarm system [3]. Each criticality monitor consists of (a) Ionization chamber, (b) Preamplifier & (c) Associated electronics for local alarm (Fig.1). System criticality alarm will annunciate only if any two criticality monitor gives alarm. Two out of three coincidence logics is chosen to reduce the probability of false alarm. This system has facilities to annunciate alarm in both the condition i.e. fast Gamma rise transient type of criticality as well as Gamma steady dose i.e. Plateau type criticality.

Distributed IO Module (DIO)

A distributed IO module with Ethernet connectivity and digital input/output channel is employed. Digital input signal is connected to the criticality monitor alarm signal available in potential free contacts. Digital output channel trigger audio visual indicators of the same laboratory. In this project micro PLCs have been used in place of distributed IO modules in distributed IO panels since it was found that Distributed IO module with Ethernet based connectivity and micro PLC module with Ethernet based connectivity do not have much difference in commercial aspects. However micro PLC module has advantages over distributed IO module as here the state of input/output during cold start can be defined. Scanning of the channel and its duration is also controllable. Schneider make TM218 series micro PLC are employed in place of distributed IO module. The input coming from existing criticality Monitor is being sensed by TM 218 Digital Input channel which is then transferred to Master control panel (M340) via Ethernet. Also the digital output for Audio visual Indicators coming from M340 is being sensed by TM218 PLC, which will turn ON Audio Visual Indicators.

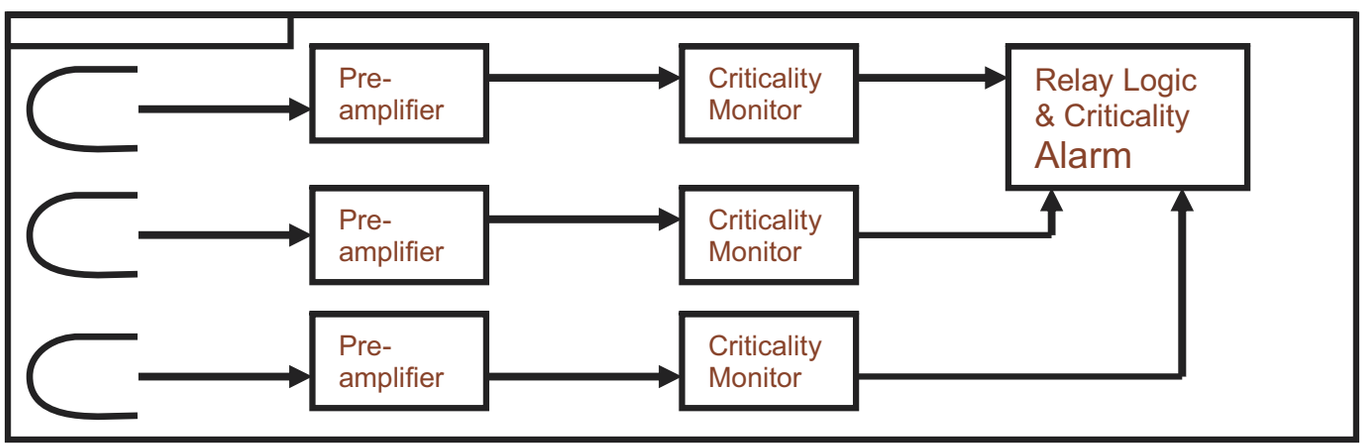

Fig. 1: Block Diagram of Criticality Alarm System

Main Controller

This is the main Control Panel which is communicating with Distributed IO Panels as well as with HMI and Annunciator panels. This panel takes the data from Distributed IO Panel (Criticality alarm input), process the data and generate output to turn ON Indications on Annunciator panels & Audio Visual Indicators. Same data is getting transferred to HMI.

IP based Window Annunciator Panel (AP)

It is a microcontroller based display units with Ethernet port which is connected to Ethernet network through RJ45 connector. Each AP is having 15 windows (13 used & 2 spare) to display the alpha-numeric characters corresponding to the room no. of the particular lab. In case of criticality the particular window will flash. Each AP is provided with hooter to give a distinguished audio output. The panel is having power-on indication and Test, Accept Push Button for Manual Operation. Annunciator Panels are provided in active and inactive corridors easily visible for the facility users. Double sided and single sided annunciator panels are used as per the locations. Total 8 nos. double sided and 7 nos. single sided annunciators are used.

Human Machine Interface

The HMI works as an annunciation device cum control console for operation of the Criticality Annunciation System. It is having Ethernet communication port for connecting to the network and another suitable port for programming with the help of a PC/Laptop. One HMI is installed in Control Room & other HMI is installed in Security Room.

Screens have been developed in the HMI for online display of overall status of detection system installed in individual room, status of all equipments connected in the criticality management system, administrative isolation of the detection instruments, provision for testing of the equipments.

Audio Visual Indicators (AVI Unit)

The AVI is beacon type flasher cum hooter. It will flash red light when activated and give distinguished audio output of about 80 dB. It is activated through relay output module of TM218 PLC. The AVIs are mounted on wall above lab room doors, HP room.

Exit Indicators

Exit Indicators are provided near entry doors and at corridors to guide the route of normal exit. There are 5 emergency exits in the facility. Emergency Exit Indicators are provided in these locations which are visible from the corresponding corridors. Normal and emergency exit indicators are having different colours of illumination and symbol. These exit indicators are powered both from normal power (Class IV 230V AC) as well as Class I (110V , DC) power with automatic switching to the available power.

Description of Scheme

The control system involves 13 Distributed IO panels for inputs from each Room, One master control panel, 7 Single sided APs, 8 Double sided APs installed in Corridors, 30 Audio Visual Indicators, 2 HMI Panels. Both the HMI's are used for supervisory and management information functions, with main controller and distributed IO panels for the continuous logic control.

All APs & AVI Units are connected to 13 Distributed IO Panels.

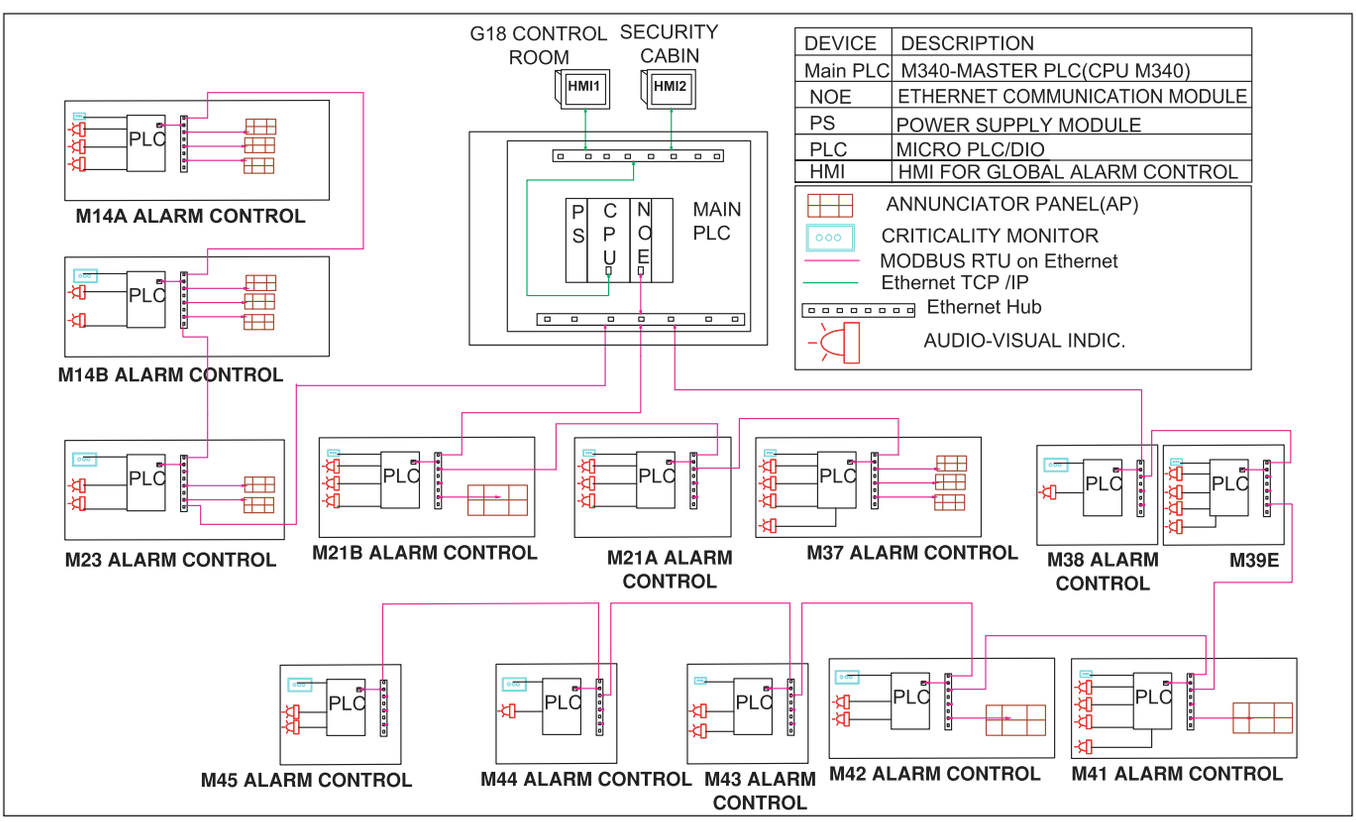

Fig. 2: Networking Scheme of Criticality Evacuation Management System

13 Distributed IO Panels are communicating with Master PLC Panel on Ethernet. The HMI stations communicate to the Master Controller over Ethernet network. There are total five Ethernet Loops used for connecting these equipments as shown in Fig. 2.

The entire system is built on the communication protocol, Modbus on Ethernet using RJ 45 Communication Port and USB Programming Port. Suitable memory and microcontrollers are used. Status LED: LED for Ethernet network Activity, processor running, LED red I/O module fault (I/O), memory card fault, processor or system fault (ERR) and Response time is Less than 60 milliseconds.

Function of Control Room HMI – To view, Accept and Reset Criticality Alarm

Function of Security HMI – To view and Accept Criticality Alarm

Basic Operating Procedure

The basic objective of the scheme is to give signal to all the staff in RMD when criticality alarm condition occurs. Whenever criticality alarm comes from any one of 13 panels, alarm input will go to all Annunciator panels, HMIs, Common AVIs & AVIs installed for particular Room.

Normally all windows of APs will be in off position and a 'power on' indication lamp for APs will be ON. All indications on HMI Main screen will be in steady Green colour. All AVI's will be in off condition.

In case of criticality alarm in any room i.e. the CM in that particular room is activated, the particular room window of all APs will flash in red colour and their hooters will sound. The same thing will be reflected in the HMI screen also. The Particular room window will start flash in red colour.

The AVIs of the lab room where the CM is activated will turn-on and the AVIs of other rooms will be in 'OFF' position except Common AVI's. Common AVI's installed in Control Room, Security Room, Health Physics Room will turn ON.

On hearing the criticality alarm, all occupants will vacate the facility through nearest emergency exit away from the lab where the criticality occurred as the affected lab room no. flashes in all Aps.

Authorized person(s) can only accept the alarm globally from HMI installed in Control Room or from Security Room. After accepting the alarm, Common AVI's, Audio Alarm i.e. Hooters of Aps will MUTE. However Video Alarm i.e. window of APs will stop flashing and become steady in Red colour. Same will be indicated in HMI also. Particular room window on HMI will show in steady Red colour. Particular room AVI's ringing, Indication on APs and HMIs will continue till the system is reset. After checking the activity, the CM is to be reset first. The Criticality Annunciation System can be reset by only authorized person(s) from any HMI located in Control Room or Security Room. After resetting the system from HMI, All windows of Annunciator panel will be OFF. All AVI' will be OFF. Also status of Windows on HMI will show in steady green colour, which will state all clear position.

Programming

In Distributed IO Panel programming, it takes input signal from CM and gets the alarm signal from main controller panel for activating AVI units connected to it. Programming is done in Ladder Logic.

Programming and screen development in HMI Panel is done under manufacturer software environment. Screens have been developed showing all room nos. as animated text and different colour.

Main Controller Panel programming is done in different sections. Alarm generation section checks input from DIO for availability of signal from CM. Whether a CM is under maintenance or in operation is logged in HMI and it is passed to controller. If CM is activated controller will generate signals for APs for visibility, audio annunciation and flash for the corresponding channel meant for the accident room. At the same time it will send signal to same DIO for activation of AVIs located on the door of the corresponding room .Authorised person after entering his authentication will be able to accept the alarm from HMI When Alarm is accepted from HMI PLC controller will stop flash and audible signal of

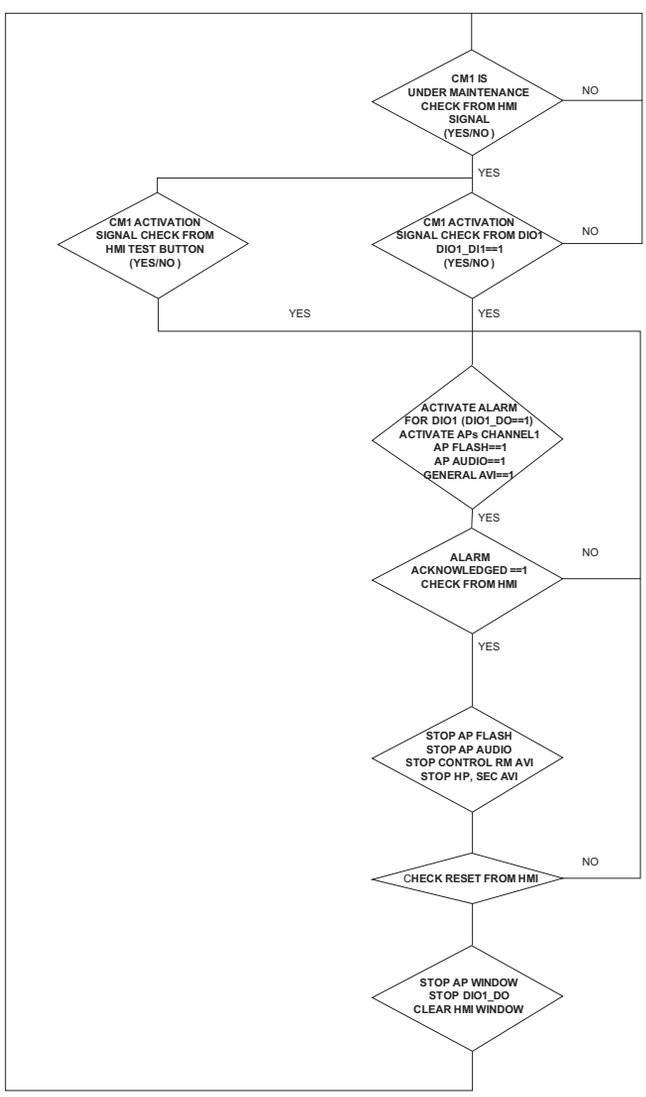

Fig. 3 : Flowchart for Alarm Logic

APs and signal will be steady. All common alarms in control rooms and security counter will stop. But the AVI signal in accident room doors will still flash and ring. When reset is pressed by authorized person from HMI , PLC controller shall send reset signal to all devices. A flow chart for the alarm activation through one DIO module is given in Fig. 3. The same program is written for all other DIOs to check other CMs and generate alarm accordingly.

Other than alarm generation program is also written to check the Ethernet communication with devices which ensures whether the devices are in working condition or not. This diagnostic data is passed to HMI for annunciation in HMI.

Screens have been developed in HMI for showing Criticality Alarm Signal (Fig. 4), Power ON status of individual Equipments (Fig. 5), test buttons, online status of connected equipments.

Fig. 4: Criticality Alarm Notification Screen

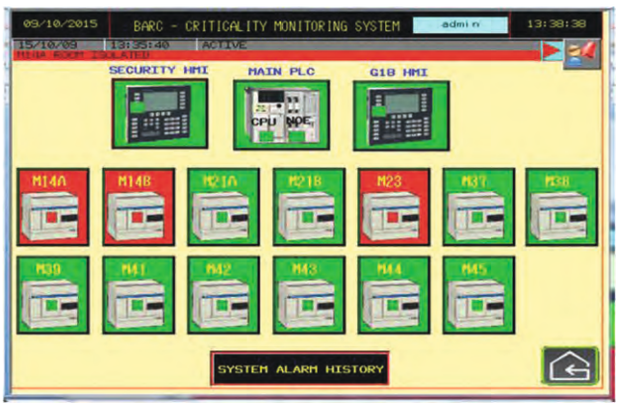

Fig. 5: Power ON Status of Equipments

Results

CMs, APs, Distributed IO panels, Main Controller Panels, HMI Stations have been installed and they have been connected vide Cat-6 Cable as per Communication Scheme in Fig 1. Photographs are enclosed herewith

Testing was done by activating CMs in each laboratory. CMs were activated by test switch and were checked in the each APs, respective AVIs, in HMI Panels at security cabin and control room. Testing includes following:

a. Activate CMs and check at individual AVIs, APS and HMIs. APS indicators shall flash and hooters shall ring.
b. Press Accept from any HMI and check window indicators at APs. It becomes steady. AVIs shall still ring .
c. Press Reset from any HMI and check window indicators at APS. It will get clears and AVIs shall also gets clear
d. Check at HMI that all events are recorded
e. Power Off any APs or any Distributed IO panel, or main controller. Indication comes to HMI about the system being power OFF
f. Test from HMI for individual CM to activate by simulation from HMI .Check accepts and reset
g. Isolate from HMI panel for any room and activate the same room from field Cms.

Testing was completed successfully and it has been found that the events get duly recorded in HMIs. Sample screenshots of

Fig. 6: Double Side AP

Fig. 7: Emergency Exit

Fig. 8: Main Controller Panel

Fig. 9: HMI Panel

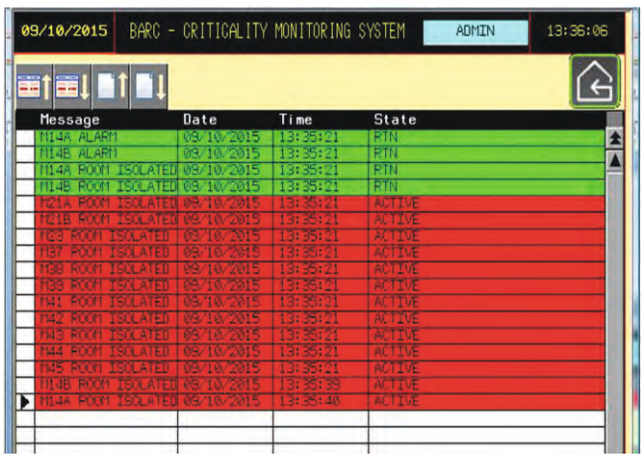

Fig. 10: Events Status in HMI Screens

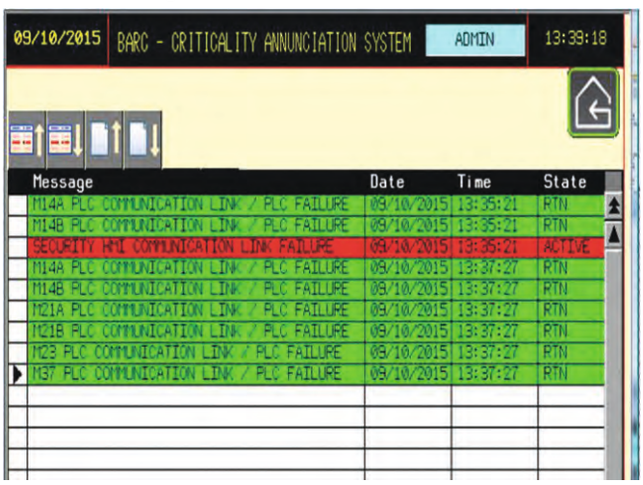

Fig. 11: Diagnostic Events Status

HMI screen is enclosed. Green colour in Fig 10 &11, shows that alarm was activated and now it is not active whereas alarm in red colour indicates that it is still active in fig 10 various reported alarms logged are shown. In fig 11 communication & power failure status of miscellaneous devices are logged with current status.

Discussion

Criticality monitoring system employed here is for prompt evacuation of the facility worker. The system is very efficient for handling alarm management. It has been noticed that existing radioactive plants employs only local alarm or few more hooters at corridors. The system described above and implemented will help the occupational worker to identify the actual and the affected room. As a result occupational worker wherever he might be seating or working will be able to escape through nearest exit paths available which is away from the affected area and highlighted in exit indicator. This will facilitate the occupational worker to exit with least radiation hazards. Criticality cannot be detected before it occurs as already explained. However the system employed here will help to reduce casualty due to criticality. The design is flexible to integrate more devices if any other laboratory is added as it is on network based. If the Annunciator or PLC or distributed IO module or the standby panel fails it will be notified in the control room. Hence frequent testing of the system would not be required. Functionality checking of the complete system by periodical basis is also easy as it is possible from the control room HMI itself. Password based accept and reset facility helps only authorized person meant for such operation can use the system.

Conclusions

The system implemented employs minimal wiring and hence is easy for a facility to maintain and easy for installation in radioactive laboratories where lot of wiring installation is difficult. Such system can be utilized in any facility consisting of large geometrical areas for safe evacuation of radiation workers with least possible of radiation hazards during criticality incidence. The new criticality warning indicators will not only alert the personnel from affected laboratory but to entire facility and will show the place of incidence from suitable distance so that evacuation can be from other direction. The components are mostly available in open market and can be customized as per the architecture of the plant. It is also possible to integrate devices which will automatically invite emergency response team to come for rescue operation.

Bibliography

1. Criticality Assessment Study and Research Department. *"Nuclear criticality risks and their prevention in plants and laboratories"*. IRSN. France: s.n., 2011. p. 16, ANALYSIS GUIDE. DSU/SEC/T/2010-334.[1]
2. International Atomic Energy Agency. *"Criticality Safety in the Handling of Fissile Material"*. s.l.: IAEA, 05 June, 2014. p. 100, Specific Safety Guide. SSG-27.[2]
3. N.K. Karnani, ED & DD, BARC et al. *"Criticality Emergencies- prevention, Detection and Development of Evacuation Alarm System in Radiological Laboratories"*. Jodhpur: s.n., 2008. Proceeding of IARPNC at Defence Laboratory.[3]
4. Internation Organizaion for Standardization (ISO). *"Nuclear Energy - Performance and testing requirements for criticality detection and alarm systems"*. s.l.: ISO, 1987. ISO7753.[4]
5. IRSN. *"Safety at basic nuclear facilities other than nuclear power plants"*. IRSN. France: s.n., 2013. Lessons learned from significant events reported in 2011 and 2012. IRSN report DG/2013-00006-EN.[5]

Central Complex at BARC

Edited & Published by:
Scientific Information Resource Division
Bhabha Atomic Research Centre, Trombay, Mumbai 400 085, India
BARC Newsletter is also available at URL:http://www.barc.gov.in